# ABSTRACT

ÖZBEK, AYSE MERVE. Measurement of Impact Ionization Coefficients in GaN. (Under the direction of B. Jayant Baliga.)

GaN has been recognized as a potential semiconductor for high temperature, high frequency and high power applications. Due to its wide bandgap, GaN exhibits high critical electric fields, which are suitable to sustain high breakdown voltages in power electronic devices. In order to obtain a good understanding of the breakdown characteristics of a power device, it is important to know the impact ionization coefficients of electrons and holes as a function of the electric field in the semiconductor.

In this work, electron and hole impact ionization coefficients have been accurately measured in both GaN epitaxial layers grown on bulk GaN substrates and GaN epitaxial layers grown on Sapphire substrates using the pulsed electron beam induced current technique. Using Chynoweth's equation ($\alpha$ = a $e^{-b/E}$), measurements for GaN epitaxial layer grown on bulk GaN substrates gave an $a_N$ value of 1.5x10$^5$ $cm^{-1}$ and a $b_N$ value of 1.413x10$^7$ V/cm for the impact ionization coefficient of electrons in GaN at room temperature. For the impact ionization coefficients of holes in GaN, the values of $a_P$ and $b_P$ were found to be 6.4x10$^5$ $cm^{-1}$ and 1.454x10$^7$ V/cm, respectively. An analytical solution of the form $\alpha = mE^n$ for the variation of the impact ionization coefficients as a function of the electric field was derived, which is useful for analytical calculation of the breakdown voltages in GaN.

For Chynoweth's equation ($\alpha$ = a $e^{-b/E}$), measurements for GaN epitaxial layers grown on Sapphire substrates gave an $a_N$ value of 9.17x10$^5$ $cm^{-1}$ and a $b_N$ value of 1.722x10$^7$ V/cm for the impact ionization coefficient for electrons at room temperature. For the impact ionization coefficients for holes at room temperature, the values of $a_P$ and $b_P$ were found to be 8.7x10$^5$ $cm^{-1}$ and 1.464x10$^7$ V/cm, respectively. The values for both coefficients are larger than those measured for GaN grown on GaN substrates.

The temperature dependence of the electron and hole impact ionization coefficients as a function of the electric field has been accurately measured for both GaN epitaxial layers grown on bulk GaN substrates and GaN epitaxial layers grown on Sapphire substrates. The impact ionization coefficients for both electrons and holes are observed to decrease with increasing temperature. This is consistent with the measured increase in the breakdown voltage with temperature for high voltage Schottky barrier diodes. This is an important observation demonstrating that stable power devices can be fabricated from Gallium Nitride.

Electron Beam Induced Current (EBIC) technique was employed in order to understand the role of defects on the breakdown characteristics of GaN. The impact ionization coefficients for electrons and holes measured at the defective site were found to be higher than those measured

at a non-defective site. These results indicate that the breakdown voltage of GaN devices can be reduced due to the presence of defects.

© Copyright 2012 by Ayse Merve Özbek

All Rights Reserved

# Measurement of Impact Ionization Coefficients in GaN

by
Ayse Merve Özbek

A dissertation submitted to the Graduate Faculty of
North Carolina State University
in partial fulfillment of the
requirements for the Degree of
Doctor of Philosophy

Electrical Engineering

Raleigh, North Carolina

2012

APPROVED BY:

| | |
|---|---|
| Mehmet C. Öztürk | Veena Misra |
| Jagdish Narayan | B. Jayant Baliga<br>Chair of Advisory Committee |

## DEDICATION

To
My Mother
Inci Özbek
and
My Father
Emin Özbek

# BIOGRAPHY

Ayse M. Özbek was born in Elazig, Turkey in February 1983. She joined Bilkent University in Ankara, Turkey in 2001. She graduated with a Bachelor of Science in Electrical and Electronics Engineering in 2006. In August 2006, she began her graduate studies in Electrical Engineering at North Carolina State University under the guidance of Prof. D. W. Barlage. Her M.S. thesis dealt with modeling of III-nitride semiconductor band devices alternative to silicon based traditional MOSFET. She continued her graduate PhD degree at North Carolina State University in the area of power semiconductor devices under the work direction of Prof. B. J. Baliga.

## ACKNOWLEDGEMENTS

The first person that I would like to thank is my supervisor Prof. B. Jayant Baliga for giving me the opportunity to work on this thesis project and providing his guidance, encouragement and support through this research.

I am grateful to Professors Veena Misra, Jagdish Narayan and Mehmet C. Öztürk for agreeing to be on my thesis committee and for their valuable suggestions and comments.

I am indebted to my colleagues for their support and encouragement. I have to give my special thanks to Edward Van Brunt, Michael Morgenson, Xiaodong Li and Rui Mao. The staff at Analytical Instrumentation Facility deserve special recognition for their assistance during the course of this work, in particular Chuck Mooney for his help with the SEM set-up. I would also like to thank Joe Matthews for his help during the processing of the devices.

Above all, I thank my parents for the much needed motivation throughout the duration of my graduate study. It was their love and support that helped me maintain sanity during stressful times. I would also like to thank Emre Alptekin, for being the ultimate source of strength and encouragement throughout my graduate study.

# TABLE OF CONTENTS

**List of Tables** . . . . . **vii**

**List of Figures** . . . . . **viii**

**Chapter 1 Introduction** . . . . . **1**
1.1 Motivation . . . . . 1
1.2 Outline of the thesis . . . . . 3

**Chapter 2 Background** . . . . . **4**
2.1 Breakdown Mechanism and Impact Ionization Coefficients . . . . . 4
2.1.1 Breakdown Mechanism . . . . . 5
2.1.2 Impact Ionization Coefficients . . . . . 5
2.2 Characterization of Impact Ionization Coefficients . . . . . 6
2.2.1 Measurement of I.I. Coefficients in Silicon . . . . . 6
2.2.2 Measurement of Impact Ionization Coefficients in 4H-SiC . . . . . 11
2.2.3 Measurement of Impact Ionization Coefficients in GaN . . . . . 14

**Chapter 3 Methodology** . . . . . **22**
3.1 Measurement Methodology . . . . . 22
3.2 Validation of the Extraction Procedure . . . . . 23
3.3 Electron Beam Penetration Depth . . . . . 26

**Chapter 4 Edge Termination of GaN Devices** . . . . . **29**
4.1 Planar, Nearly Ideal Edge Termination Technique for GaN Devices . . . . . 30
4.1.1 Fabrication . . . . . 30
4.1.2 Electrical Characterization . . . . . 31
4.1.3 Results and Discussion . . . . . 32
4.2 Finite Zone Argon Implant Edge Termination for High Voltage GaN Schottky Rectifiers . . . . . 33
4.2.1 Fabrication . . . . . 34
4.2.2 Results and Discussion . . . . . 35

**Chapter 5 Electron Beam Induced Current (EBIC) Technique** . . . . . **40**
5.1 Scanning electron microscopy . . . . . 40
5.2 EBIC Technique . . . . . 41
5.3 EBIC Study of Edge Termination . . . . . 43
5.3.1 Unterminated Diodes . . . . . 43
5.3.2 Argon Ion Implant Terminated Diodes . . . . . 44

**Chapter 6 Measurement of Impact Ionization Coefficients for GaN . . . . . 46**
6.1 Experimental Setup . . . . . 47
6.2 Measurement of Impact Ionization Coefficients for GaN Epilayer Grown on Bulk GaN Substrate . . . . . 49
6.2.1 Device Fabrication and Characterization . . . . . 49
6.2.2 Impact Ionization Data . . . . . 49
6.2.3 Discussion of experimental results . . . . . 51
6.2.4 Application of extracted impact ionization data . . . . . 52
6.3 Measurement of Impact Ionization Coefficients for GaN Epilayer Grown on Sapphire Substrate . . . . . 58
6.3.1 Device Fabrication and Characterization . . . . . 58
6.3.2 Impact Ionization Data . . . . . 59
6.4 Comparison of Impact Ionization Data for GaN . . . . . 59
6.5 Role of Defects on Impact Ionization in GaN . . . . . 60
6.6 Temperature dependence of impact ionization coefficients in GaN . . . . . 63

**Chapter 7 Conclusion and Future Work . . . . . 70**

**References . . . . . 72**

## LIST OF TABLES

Table 4.1 Comparison of BFOM for GaN with Silicon and Silicon Carbide . . . . . 33

## LIST OF FIGURES


Figure 2.1 Ionization rate versus electric field for Silicon from P. A. Wolff, "Theory of Electron Multiplication in Silicon and Germanium", Phys. Rev., vol. 95, pp. 1415, 1954 [25] . . . . . 7

Figure 2.2 Circuit used for obtaining the multiplication characteristics for Silicon from A. G. Chynoweth and K. G. McKay, "Threshold Energy for Electron-Hole Pair Production by Electrons in Silicon", Phys. Rev., vol. 108, pp.29, 1957 [27] . . . . . 8

Figure 2.3 Fit of the electron ionization data for Silicon to one of Baraff's curves for junctions with breakdown voltages ranging from 6 to 95 V from C. A. Lee et. al., "Ionization Rates of Holes and Electrons in Silicon", Physics. Review, vol. 134, pp. 761, 1964 [34] . . . . . 10

Figure 2.4 Measured avalanche coefficient (data points) for two samples and the fitting curve to Baraff theory calculation (solid line) for 6H-SiC from G. H. Glover, "Charge multiplication in Au-SiC (6H) Schottky junctions", Journal of Applied Physics, vol. 46, pp. 4842, 1975 [36]. . . . . 12

Figure 2.5 Impact Ionization rates for electrons and holes in 4H SiC from A. O. Konstantinov, "Study of Avalanche Breakdown and Impact Ionization in 4H Silicon Carbide", Journal of Electronic Materials, vol. 27, pp. 335, 1998 [38]. . . . . 14

Figure 2.6 SiC Impact Ionization Coefficient for electrons from A. O. Konstantinov et. al., "Study of Avalanche Breakdown and Impact Ionization in 4H Silicon Carbide", Journal of Electronic Materials, vol. 27, pp. 335, 1998 [38] (∘), T. Hatakeyama et. al.,"Impact Ionization Coefficient of 4H Silicon Carbide", Applied Physics Letters, vol. 85, pp. 1380, 2004 [40] ( △) and W. S. Loh et. al., "Impact Ionization Coefficients in 4H-SiC", IEEE Transactions on Electron Devices, vol. 55, pp.1984, 2008 [41] (□). . . . . 15

Figure 2.7 SiC Impact Ionization Coefficient for holes from A. O. Konstantinov et. al., "Study of Avalanche Breakdown and Impact Ionization in 4H Silicon Carbide", Journal of Electronic Materials, vol. 27, pp. 335, 1998 [38] (∘), R. Raghunathan and B. J. Baliga, "Role of defects in producing negative temperature dependence of breakdown voltage in SiC", Applied Physics Letters, vol. 72, pp. 3196, 1998 [39] (×) T. Hatakeyama et. al.,"Impact Ionization Coefficient of 4H Silicon Carbide", Applied Physics Letters, vol. 85, pp. 1380, 2004 [40] ( △) and W. S. Loh et. al., "Impact Ionization Coefficients in 4H-SiC", IEEE Transactions on Electron Devices, vol. 55, pp.1984, 2008 [41] (□). . . . . 15

Figure 2.8 Electron Impact Ionization Coefficient for Wurtzite GaN from (□) J. Kolnik et. al., "Monte Carlo calculation of electron initiated impact ionization in bulk zinc-blende and wurtzite GaN", Journal of Applied Physics, vol. 81, 1997 [11], (∘), F. Bertazzi et. al., "Theory of high-field carrier transport and impact ioinization in wurtzite GaN. Part 1: A full band Mote Carlo model", Journal of Applied Physics, vol. 16, 2009 [15], (∗), J. C. Cao and X. L. Lei, "Nonparabolic multivalley balance-equation approach to impact ionization: Application to wurtzite GaN", European Physics Journal, vol. 7, pp. 7983, 1999 [13] and S. Chen and G. Wang, " High-field properties of carrier transport in bulk wurtzite GaN: A Monte Carlo perspective", Journal of Applied Physics, vol. 7, 2008 [14] (◊). . . . 17
Figure 2.9 Hole Impact Ionization Coefficient for Wurtzite GaN by (∘), F. Bertazzi et. al., "Theory of high-field carrier transport and impact ioinization in wurtzite GaN. Part 1: A full band Mote Carlo model", Journal of Applied Physics, vol. 16, 2009 [15] and S. Chen and G. Wang, " High-field properties of carrier transport in bulk wurtzite GaN: A Monte Carlo perspective", Journal of Applied Physics, vol. 7, 2008 [14] ( ◊). . . . . 17
Figure 2.10 Impact Ionization Coefficients for Zinc-blende GaN by (□) J. Kolnik et. al., "Monte Carlo calculation of electron initiated impact ionization in bulk zinc-blende and wurtzite GaN", Journal of Applied Physics, vol. 81, 1997 [11] and (+) I. H. Oguzman et. al., "Theory of hole initiated impact ionization in bulk zincblende and wurtzite GaN", Journal of Applied Physics, vol. 81, 1997 [12]. . . . . 18
Figure 2.11 Structure of the AlGaN/GaN HJFET from K. Kunihiro et. al., "Experimental Evaluation of Impact Ionization Coeffients in GaN", IEEE Electron Device Letters, vol. 20, 1999 [16]. . . . . 19
Figure 2.12 DC Characteristics of the AlGaN/GaN HJFET, a)Ig versus Vd, b)Id versus Vd from K. Kunihiro et. al., "Experimental Evaluation of Impact Ionization Coeffients in GaN", IEEE Electron Device Letters, vol. 20, 1999 [16] . . . . . 20
Figure 2.13 Impact Ionization coefficients in GaN extracted from the gate current at Vg=0 V of the AlGaN/GaN HJFET, where Leff=0.4 $\mu$m is assumed from Monte Carlo simulation results from K. Kunihiro et. al., "Experimental Evaluation of Impact Ionization Coeffients in GaN", IEEE Electron Device Letters, vol. 20, 1999 [16]. . . . . 21

Figure 3.1 Device structure used for numerical simulations . . . . . 24
Figure 3.2 The electric field profile obtained from simulations showing that a nearly constant electric field occurs in the drift region . . . . . 25
Figure 3.3 Extraction of $\alpha_n$ is possible by using excitation confined near the Schottky contact($t_{ex}$=0.05 $\mu$m). . . . . 25
Figure 3.4 Extraction of $\alpha_p$ is possible by excitation throughout the drift region of the Schottky diode($t_{ex}$=4 $\mu$m). . . . . 26

Figure 3.5 Effect of excitation thickness on the extracted impact ionization coefficients. The symbols show the extracted values for the impact ionization coefficients. . . . . 27
Figure 3.6 Impact of excitation thickness on the extracted impact ionization coefficients for an electric field of $2 \times 10^6$ V/cm in the drift region. . . . . 27
Figure 3.7 Penetration Depth versus Electron Beam Energy . . . . . 28

Figure 4.1 a)Structure of the fabricated diode, b) Structure of the shadow mask. . . 30
Figure 4.2 Carrier Density($cm^{-3}$) vs. W profile . . . . . 31
Figure 4.3 Breakdown voltage measurements for a)unterminated Schottky diode and b)Implant Dose:2x$10^{16}$ $cm^{-3}$ . . . . . 32
Figure 4.4 Breakdown voltage shown as the function of implant dose on the edges of Schottky barrier diodes. . . . . 33
Figure 4.5 Forward IV characteristics for a)unimplanted Schottky diode and b)implanted Schottky diode. . . . . 34
Figure 4.6 Cross section of the fabricated GaN Schottky barrier diodes. . . . . 35
Figure 4.7 Back-to-back Schottky diode . . . . . 36
Figure 4.8 Measured reverse current voltage characteristics for terminated GaN Schottky barrier structures with various implant region lengths. . . . . 37
Figure 4.9 Experimental data on dependence of breakdown voltage on edge termination length. . . . . 37
Figure 4.10 Experimental data on increase in leakage current of terminated structure with increasing implant region length. . . . . 38
Figure 4.11 Electric Field obtained using Numerical Simulations for terminated structure as a function of implant region length . . . . . 38
Figure 4.12 Simulation results of breakdown voltage dependence on edge termination length. . . . . 39

Figure 5.1 Schematic of the experimental setup of EBIC Measurements . . . . . 42
Figure 5.2 EBIC line scan on unterminated GaN Schottky Barrier Diode . . . . . 43
Figure 5.3 EBIC image of an unterminated GaN Schottky diode at a reverse bias of -75V and -100V at room temperature . . . . . 44
Figure 5.4 EBIC image of a terminated GaN Schottky diode at a reverse bias of 75 V at room temperature. . . . . 45

Figure 6.1 Schematic of the experimental setup . . . . . 48
Figure 6.2 Measured multiplication factor with increasing reverse bias on the GaN Schottky diode. . . . . 50
Figure 6.3 Measurement of repeatability in extraction of impact ionization coefficients. 51
Figure 6.4 Effect of electron beam energy on the measured impact ionization coefficients in GaN. . . . . 52
Figure 6.5 Measured impact ionization coefficients for electrons and holes in GaN using data taken at 10 diodes. . . . . 53

Figure 6.6 Comparison of measured impact ionization coefficients for electrons and holes in GaN at room temperature with the previous values reported in literature. . . . . 54
Figure 6.7 Power law approximations for the impact ionization coefficients in GaN and SiC. . . . . 55
Figure 6.8 Comparison of critical electric fields for breakdown in GaN, SiC and Si. . 56
Figure 6.9 Comparison of breakdown voltages for GaN, SiC and Si. . . . . 56
Figure 6.10 Comparison of depletion layer width at breakdown in GaN, SiC and Si. . 58
Figure 6.11 Ideal Specific On-resistance for the drift region for unipolar devices in GaN, SiC and Si. . . . . 58
Figure 6.12 Measured impact ionization coefficients for electrons and holes in GaN using data taken at 10 diodes at room temperature. . . . . 60
Figure 6.13 Comparison of the measured impact ionization coefficients for electrons and holes in GaN at room temperature with the previous values reported in literature. . . . . 61
Figure 6.14 Impact Ionization coefficients for electrons in GaN measured at a defect site compared to those measured at defect-free location. . . . . 62
Figure 6.15 Impact Ionization coefficients for holes in GaN measured at a defect site compared to those measured at defect-free location. . . . . 62
Figure 6.16 Measured electron impact ionization coefficients for GaN epitaxial layer grown on bulk GaN substrate at temperatures ranging from 300 K to 375 K. . . . . 64
Figure 6.17 Measured hole impact ionization coefficients for GaN epitaxial layer grown on bulk GaN substrate at temperatures ranging from 300 K to 375 K. . . 65
Figure 6.18 Temperature dependence of the coefficients $a_n$ and $a_p$ for GaN epitaxial layer grown on bulk GaN substrate. . . . . 65
Figure 6.19 Temperature dependence of the coefficients $b_n$ and $b_p$ for GaN epitaxial layer grown on bulk GaN substrate. . . . . 66
Figure 6.20 Measured electron impact ionization coefficients for GaN epitaxial layer grown on Sapphire substrate at temperatures ranging from 300 K to 375 K. 66
Figure 6.21 Measured hole impact ionization coefficients for GaN epitaxial layer grown on Sapphire substrate at temperatures ranging from 300 K to 375 K. . . . 67
Figure 6.22 Temperature dependence of the coefficients $a_n$ and $a_p$ for GaN epitaxial layer grown on sapphire substrate. . . . . 67
Figure 6.23 Temperature dependence of the coefficients $b_n$ and $b_p$ for GaN epitaxial layer grown on sapphire substrate. . . . . 68
Figure 6.24 Measured increase of breakdown voltage with increasing temperature for both GaN epitaxial layer grown on bulk GaN substrate and GaN epitaxial layer grown on Sapphire substrate. . . . . 69

# Chapter 1

# Introduction

Power semiconductor devices are a key component of all power electronic systems. It is estimated that as much as 50 percent of the electricity used in the world is controlled by power devices. Power devices have a major impact on the economy, because they determine the cost and efficiency of most electrical systems. Power semiconductor devices have taken a dominant role with silicon serving as the base material after replacing vacuum tubes by solid state devices [1]. Bipolar power devices, such as bipolar transistors and thyristors, were first developed in the 1950s. Their power ratings and switching operating frequencies increased with better understanding of the operating physics and availability of more advanced lithographie techniques [1]. The power MOSFET has become the device of choice due to its inherent high switching speed and its high input impedance under steady state conditions [2]. However, in order to minimize the power losses in power MOSFETs, the on resistance should be reduced, which can be achieved by increasing the device die area and by reducing the specific on resistance. Therefore, other semiconductor materials are considered to have further improvements in device performance. In the early 1980s, replacing silicon with wide band-gap semiconductors was suggested. The basis of this approach is based on the Figure of Merit equations [3]. The physical properties of Gallium Nitride (GaN), high saturation velocity, high breakdown fields, high electron mobility, wide bandgap energy and high thermal conductivity make it a promising material for high speed, high power, and high frequency applications [4].

## 1.1 Motivation

Gallium Nitride is a promising material for high-voltage and high temperature devices due to its remarkable material properties like wide bandgap (3.4 eV), large critical electric field (3.7 MV/cm) and a high saturation velocity ($1.9 \times 10^7$ cm/s ) [5]. In addition to its good characteristics, alloys of GaN are also utilized in device engineering. InGaN and AlGaN materials offer

a wide range of band gap 0.8 eV to 6.2 eV. This enables the design and fabrication of novel devices.

As the Si CMOS scaling continues, the short channel effect is getting more pronounced. GaN is also a potential candidate for very short channel devices due to its material properties such as its large band gap, high saturation velocity and high thermal conductivity [5]. GaN also has an advantage over Si, because it can suppress the source/drain leakage, supporting larger drive current, and eases the restriction of the device cooling [6].

An important distinction in gallium nitride is the difference between heteroepitaxial and homoepitaxial growth. When GaN is heteroepitaxially grown on non-native substrates such as sapphire, silicon or 4H-silicon carbide (4H-SiC). The defect densities in these substrates are generally high ($10^8$ - $10^10$ $cm^{-2}$) due to the lattice mismatch between the substrate and the epitaxial-grown GaN as well. Yet, recent development on GaN substrates allows thicker films and homoepitaxial growth, yielding lower defect densities ($10^6$ - $10^8$ $cm^{-2}$) [7][8][9].

This distinction causes ambiguity in material parameters with large discrepancies between hetero- and homoepitaxial GaN breakdown electric field, saturation electron velocity, and thermal conductivity values. Breakdown field and saturation velocity values are specifically impacted by defects while thermal conductivity is simply due to the non-native substrate having poor thermal conductivity [10].

If GaN is to be widely used as the semiconductor for fabricating power devices. It is essential that the parameters governing its electrical performance to be determined accurately. One of the most important parameters of a GaN power device is its breakdown voltage. In order to obtain a clear understanding of its breakdown characteristics, it is important to know the impact ionization coefficients of GaN. It is also important that the breakdown voltage of a device increase with temperature for it to have stable reliable behavior. This again is determined by the variation of impact ionization coefficients with temperature. The impact ionization coefficients not only determine the reverse bias characteristics of a device but they also influence the forward characteristics. Hence, it is important to have a good understanding of the impact ionization coefficients and their variation with temperature.

However, there is very little information on impact ionization coefficients available in literature for GaN [11][12][13][14][15][16][17] and more so on its variation with temperature. Also, there has been contradictory reports in the literature on the variation of breakdown voltage with temperature. Earlier reports by Tan et. al. [18], Johnson et al. [20] and Zhong et al. [21] indicated a negative temperature coefficient for breakdown in GaN. However, Dykonova et al. [19] and Dmitriev et al. [22] indicate positive temperature coefficients for breakdown in GaN.

The aim of this work is to measure the impact ionization coefficients for electrons and holes accurately for GaN. Also, the role of defects and temperature on the variation of breakdown voltage of GaN devices has been investigated. These results are expected to have widespread

utility for GaN device analysis and design.

## 1.2 Outline of the thesis

The thesis consists of five chapters.

Chapter 1 contains the introduction for the thesis and the motivation of measurement of impact ionization coefficients in GaN .

Chapter 2 contains the background information about the measurement methods of impact ionization coefficients in Silicon and Silicon Carbide. This chapter also summarizes the previous works from the literature on the measurement of the impact ionization coefficients in GaN.

Chapter 3 explains the measurement methodology to measure the impact ionization coefficients in GaN throughout this study.

Chapter 4, a planar edge termination technique based on creating defects some of which are expected to be located near the mid-gap of GaN is discussed. Using this termination technique, ideal parallel plane breakdown voltages were achieved.

Chapter 5 explains the Electron Beam Induced Current technique. This chapter also contains the EBIC study to observe the effect of edge termination technique.

Chapter 6 contains the measurement set-up and measurement results of the electron and hole impact ionization coefficients in GaN epitaxial layer grown on bulk GaN substrate and GaN epitaxial layer grown on Sapphire substrate. Equations derived from the impact ionization coefficients for analytical calculation of breakdown voltages in GaN. This chapter also contains the role of defects on the impact ionization data and the effect of temperature on the impact ionization coefficients.

Finally, Chapter 7 contains the discussions regarding this work and future research directions are explained in this chapter.

# Chapter 2

# Background

Power semiconductor devices play a crucial role in the regulation and distribution of power and energy in the world. Power devices are designed to be able to control the high voltage and currents required for the power electronic systems such as power supplies, automotive electronics,etc. Most unique feature of power semiconductor devices is their ability to withstand high voltages. Therefore, the fundamental parameter of these devices that governs the electrical performance is their breakdown voltage. In order to obtain a clear understanding of their breakdown characteristics, it is important to know the impact ionization coefficients.

## 2.1 Breakdown Mechanism and Impact Ionization Coefficients

The breakdown voltage of a power device is one of its most important characteristics. Together with its maximum current handling capability, this parameter determines the power rating of a device. Depending on the application, the breakdown voltage of power devices can range from 20 to 30 V for voltage regulator modules used to deliver power to microprocessors in personal computers and serves to over 5,000 V for devices used in power transmission networks [2]. The voltage is supported by a depletion layer formed across either a P-N junction, a metal semiconductor interface (Schottky barrier) interface or a metal oxide-semiconductor (MOS) interface in power devices. The high electric field that exists inside the depletion layer is responsible for sweeping out any holes and electrons that exist in this region, by either space charge generation or by diffusion. This current is small and these devices exhibit a small, nearly voltage-independent saturation current under reverse bias. However, after the critical reverse bias voltage for breakdown ($V_{BR}$) is applied, the reverse current increases sharply and relatively large currents can flow with little further increase in voltage.

### 2.1.1 Breakdown Mechanism

Breakdown can occur by two mechanisms, each of which requires a critical electric filed in the junction transition region. The first mechanism is called the Zener effect. When a heavily doped junction is reserve biased, the energy bands overlap at relatively low voltages. This leads to alignment of a large number of empty states in the n-side conduction band across the many filled states of the p-side valence band. If the barrier separating the two bands is narrow, tunneling of electrons can occur. The tunneling contributes to the reverse bias current and is called the Zener effect. As the reverse bias is increased, the barrier between the two bands becomes smaller. As the barrier becomes smaller and the reverse bias current increases. Finally, the device undergoes Zener breakdown at low reverse biases.

The second breakdown mechanism is the avalanche breakdown. For lightly doped junctions, electron tunneling is negligible and the breakdown mechanism involves the impact ionization of host atoms by energetic carriers. As the applied voltage is increased, electric field in the depletion region increases. The increase in the electric field results in acceleration of the mobile carriers to higher velocities. At sufficiently high electric fields, these carriers have sufficient energy that their collision with the atoms in the lattice can excite valence band electrons into the conduction band. The process of electron-hole pair generation due to the energy gained from the high field in the semiconductor is called impact ionization (I.I). Electron-hole pairs that are generated by the impact ionization undergo acceleration by the existing electric field and they also participate in the creation of further electron-hole pairs. Therefore, impact ionization is a multiplicative process that leads to a cascade of mobile carriers transported through the depletion region leading to a significant current flow through it. Due to the rapid increase in current, device can not sustain the application of higher voltages and undergoes avalanche breakdown.

### 2.1.2 Impact Ionization Coefficients

The creation of electron-hole pairs as a result of carrier colliding with the crystal lattice is called impact ionization. To characterize the impact ionization process, it is useful to define the impact ionization coefficients. The impact ionization coefficients for electrons is defined as the number of electron-hole pairs created by an electron traversing 1 cm through the depletion region along the direction of the electric field. Similarly, the impact ionization coefficients for holes is defined as the number of electron-hole pairs created by a hole traversing 1 cm through the depletion region along the direction of the electric field.

## 2.2 Characterization of Impact Ionization Coefficients

### 2.2.1 Measurement of I.I. Coefficients in Silicon

Avalanche multiplication of carriers in reverse biased Silicon p-n junctions have been studied extensively. McKay and McAfee first demonstrated that it is possible to obtain charge multiplication by injecting charge carrier into a Silicon p-n junction under high field conditions [23]. They measured the multiplication value by illuminating a p-n junction. They first measured the voltage-current data of the non-illuminated junction and then they measured the voltage-current data of the illuminated junction. The multiplication data was calculated by dividing the current value for the illuminated junction by the current value for the non-illuminated junction for the same voltage value. It was also assumed that both electrons and holes multiply at the same rate. The minimum energy to create electron-hole pairs was also given as between 1.1 eV and 3.6 eV as a result of alpha bombardment measurements.

McKay applied a considerable part of the gas discharge theory to the solid state case [24]. By using the formulas of the Townsend's $\beta$ mechanism, he derived the values of the ionization rates per unit length, $\alpha_i$, from the data. Making the assumption that the ionization rates for holes and electrons were equal, McKay was able to deduce the field dependence of the ionization rates.

Wolff had made a theoretical calculation of the $\alpha_i$ vs. electric field by solving the Boltzmann's transport equation [25]. In this work, Wolff has accounted for the various forces and interactions that can affect the state of motion of electrons or holes within the solid. The analysis is as follows: Particles moving in a high field are accelerated by the field. In addition, they interact with the lattice vibrations of the crystal, emitting and absorbing photons in a such a way that the net effect is a resistive or a frictional opposing the accelerating field. Finally, when the electrostatic field is high enough, they reach sufficient energy to produce electron-hole pairs in collisions with valence electrons. Experiments of Ryder and Shockley indicate that the fast electrons lose energy principally to the optical modes of the lattice. Wolff assumed that the mean free path for collisions between electrons and optical phonons is constant. Having made this assumption, he describes the methodology used to solve the Boltzmann's distribution function, which depends on the magnitude and the direction of the electron velocity. The impact ionization coefficient $\alpha_E$ was found as:

$$\alpha_E = \exp(-3E_r E_i / qE\lambda) \tag{2.1}$$

where $E_r$ is the optical photon energy, $E_i$ is the threshold energy for ionization and $\lambda$ is the mean free path for the optical phonon scattering of energetic carriers, q is the electronic charge and E is the electric field. In regions with low electric filed, only those carriers that do not suffer any

phonon scattering are able to reach the threshold and contribute to the production of electron-hole pairs. The plot of ($\alpha$/cm) versus electric filed for silicon from Wollf's predictions is shown in Figure 2.1. McKay and McAfee's data is in good agreement with the Wolff's theory in the high field region; but poor in low field region. Wolff had concluded that there is no simple expression for a $\alpha_i$ as a function of electric filed; but numerical calculations show that the general form of the curve is determined by the factor $\exp(-E/W)$, where W= $((e\varepsilon\lambda)^2)/(3(1-\cos(\theta))*hw))$.

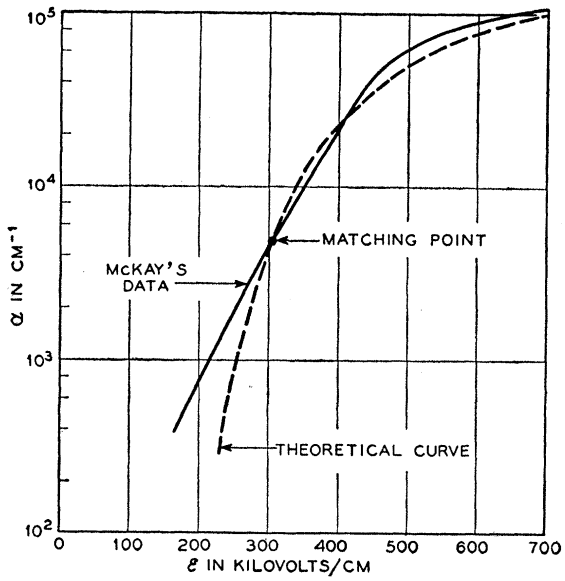


Figure 2.1: Ionization rate versus electric field for Silicon from P. A. Wolff, "Theory of Electron Multiplication in Silicon and Germanium", Phys. Rev., vol. 95, pp. 1415, 1954 [25]

Miller had been able to solve the analytical expressions for the multiplication for the case where the ionization rates for holes and electrons are different [26]. The measurements are done by injecting carriers on the high resistivity side of the step junction by means of light irradiation using p+n and n+p diodes. It was observed that the ionization rate of electrons is higher than the ionization rate of holes. Miller also measured the threshold energy for pair production as 1.5 eV for electrons and 3.5 eV for holes.

Chynoweth and McKay measured the energy an electron must have to create electron hole pairs [27]. Their method was based on varying the bias across a p-n junction gradually and determine the potential across the junction at which charge multiplication was observed to begin by using the circuit shown in Figure 2.2. Using this set-up, they reported multiplication values as low as 1.005 and calculated the threshold energy for an electron-hole pair production as 2.25 eV.

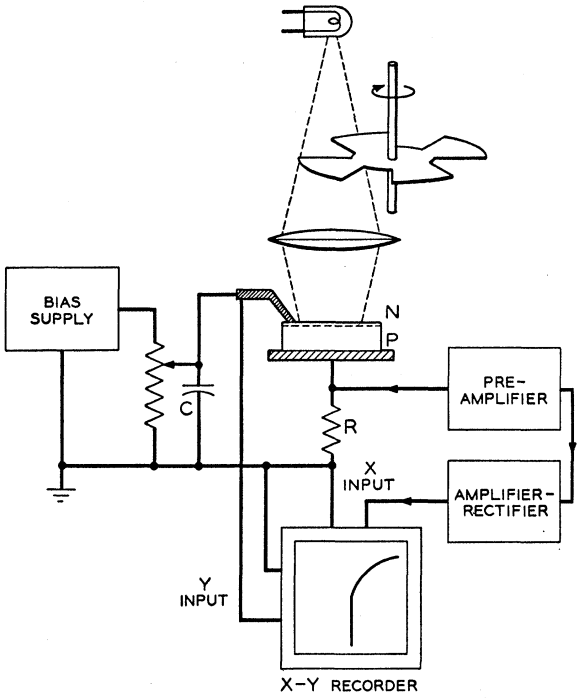


Figure 2.2: Circuit used for obtaining the multiplication characteristics for Silicon from A. G. Chynoweth and K. G. McKay, "Threshold Energy for Electron-Hole Pair Production by Electrons in Silicon", Phys. Rev., vol. 108, pp.29, 1957 [27]

Chynoweth, using more refined techniques, measured M versus bias for individual junctions over much wider ranges of field [28]. His analysis showed that the ionization rates for electrons and holes, $\alpha$ and $\beta$,followed laws of the form: $\alpha$=a exp(-b/E), where a and b are constants. He concluded that the constants a and b are different for electrons and holes. However, Wollf's theory [25],which was the existing theory at that time, did not lead to a $E^{-1}$ dependence of an exponential factor, suggesting that some fresh theoretical approach is needed.

Chynoweth and Pearson showed that dislocations acted as preferred sites for avalanche breakdown in silicon, and they suggested that a tendency toward a linear carrier motion along the direction of the field might be promoted by the band gap distortions produced by a dislocation [29]. To understand the effect of dislocation on breakdown mechanism, Chynoweth performed measurements on dislocation fee junctions and compared the data to the already existing data that apply to junctions in which breakdown is made easier by the presence of defects [30]. Measurements showed that the ionization rates for a uniform junctions are lower than than those of junctions with dislocations. However, the ionization rate has the same sort of field dependence of $\alpha$=a exp(-b/E) over most of the field range covered in these junctions. He also concluded that there was a need for some fresh theoretical approach to understand avalanche breakdown.

The phenomenon of secondary ionization, avalanche breakdown and microplasma phenomenon in p-n junctions were analyzed by Shockley, using a simplified model in which electron and holes have identical properties described by four constants [31]. Only two scattering processes for carriers are considered, each having 2 constants: generation of highest energy and ionization or electron hole production. The probability that a carrier introduced into the crystal can produce ionization before dissipating energy E-$E_i$ to phonons and becoming unable to ionize is the main difference between Shockley's and Wolff's model. $E_i$ is the threshold energy to produce an electron-hole pair. In order to loose energy, it must take:

$$C = (E - E_i)/E_R \tag{2.2}$$

where C is the number of collisions with the phonons and $E_R$ is the energy of phonons. Probability of ionizing on the average distance $CL_R$ is:

$$P(E) = 1 - exp(-(E - E_i/r_R). \tag{2.3}$$

Shockley concluded that his model predicts that impact ionization coefficient varies with field:

$$\alpha(F) = (qF/rE_R)exp(E_i/(qFL_R). \tag{2.4}$$

Baraff calculated the impact ionization coefficients in silicon using an approach that relies

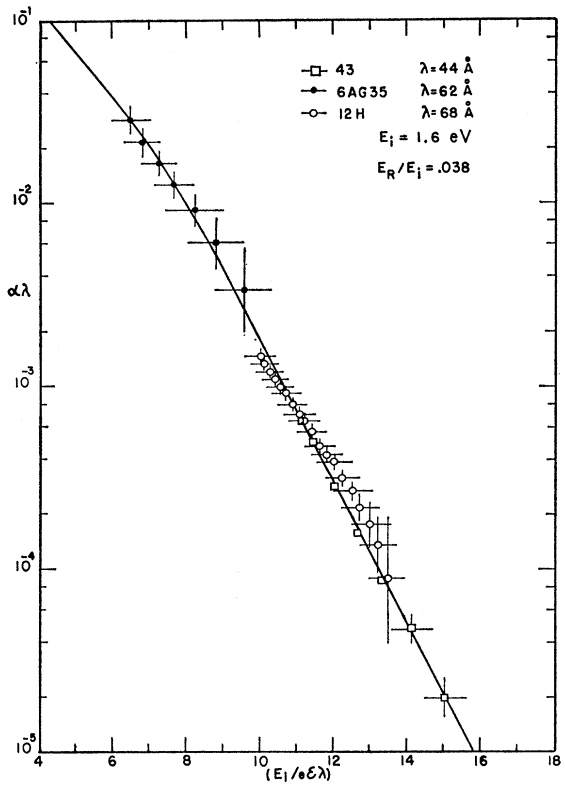


Figure 2.3: Fit of the electron ionization data for Silicon to one of Baraff's curves for junctions with breakdown voltages ranging from 6 to 95 V from C. A. Lee et. al., "Ionization Rates of Holes and Electrons in Silicon", Physics. Review, vol. 134, pp. 761, 1964 [34]

neither on the diffusion approximation followed by Wolff nor the spike approximation followed by Shockley [32]. He made such an approach in order to determine the ionization coefficients in the intermediate electric field regions where the fields were not high enough to maintain the nearly symmetrical distribution assumed by Wolff nor was it to low enough to render the high energy tail of the distribution sharply peaked in the forward direction as assumed by Shockley. The approach was made through an integral equation for the collision density. He obtained a plot of $\alpha$ versus E for Silicon and he concluded that at the field of interest, the distribution of electrons is not as symmetrical as it should be for the approximation of Wolff to apply nor it is the spike that Shockley suggested either. The approach followed by Baraff was confirmed by Lee et al. [34] later as shown in Figure 2.3.

Moll and Van Overstraeten computed the filed dependence of the ionization rates for electrons and holes from the measurement of charge multiplication in silicon p-n junctions [33].

The ionization rates that they calculated satisfy Chynoweth's law and approximated by:

$$\alpha_{(E)} = 7.03x10^5 exp(-1.231x10^6/E)cm^{-1} \tag{2.5}$$

for E between 1.75x10$^5$ Vcm$^{-1}$ and 6.4x10$^5$ Vcm$^{-1}$

$$\beta_{(E)} = 1.582x10^6 exp(-2.036x10^6/E)cm^{-1} \tag{2.6}$$

for E between 1.75x10$^5$ Vcm$^{-1}$ and 4x10$^5$ Vcm$^{-1}$.

### 2.2.2 Measurement of Impact Ionization Coefficients in 4H-SiC

Silicon Carbide received increasing attention for high power, high temperature and high frequency applications. Some of the features that make silicon carbide attractive is its wide bandgap (3.26 eV), large critical electric field strength, large thermal conductivity and a reasonable high electron mobility.

Van Opdorp and Vrakking investigated the reverse I-V characteristics of epitaxial 6H-SiC for the first time [35]. They calculated breakdown fields for SiC p-n junctions from C-V measurements and reported that the largest value found for the maximum field at breakdown is 5x10$^6$ V/cm. They reported that after electrolytic etching the junctions in a mixture of HF, alcohol and water showed sharp breakdown.

Glover reported the first measurements of the avalanche ionization rate in SiC [36]. He used Schottky junctions formed on single-crystal n-type 6H-SiC and Gold (Au) was used as the Schottky contact. Glover also observed the sharp breakdown characteristics after the chemical etching of the samples. He calculated the doping profile of the samples from the C-V characteristics. Chopped monochromatic light was used to generate the carriers in the Schottky contact and the ionization rates were determined by measuring the generated photocurrent as a function of the reverse bias voltage. The ionization rate was calculated using the assumption of equal electron and hole rates. Glover states that even if this assumption is not valid, the results will in some sense be an effective avalanche characteristic which is useful for calculating breakdown fields. Glover made measurements on two different samples with different doping concentrations and the impact ionization data obtained from both measurements are shown to fit Baraff's theory very well [32] as shown in Figure 2.4. The critical electric field value obtained from this data was 1x10$^6$ V/cm, which was much lower than the value reported by C.V. Opdorp et al [35].

Raghunathan and Baliga et al. used a impact ionization coefficients measurement method that was based upon the multiplication of carriers generated by a pulsed electron beam in the depletion region of a reverse biased diode [37]. Electron beam with a spot size of less than 20 $\mu$m

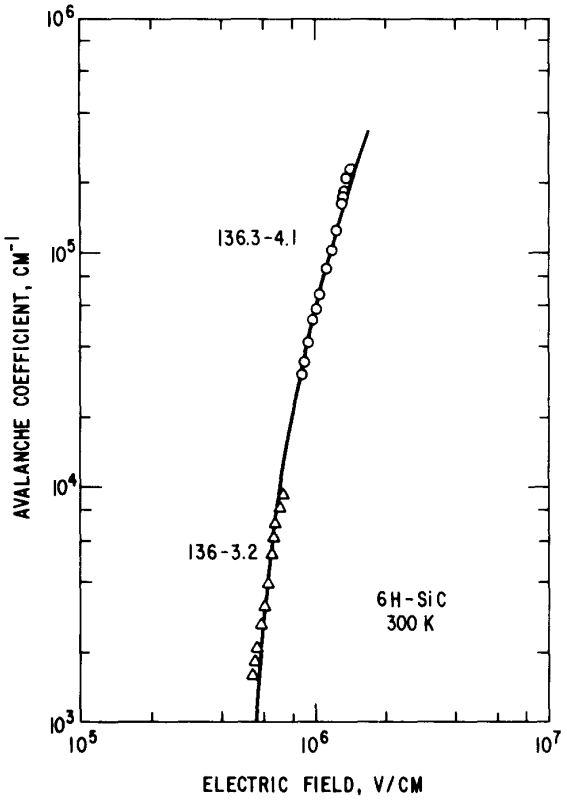


Figure 2.4: Measured avalanche coefficient (data points) for two samples and the fitting curve to Baraff theory calculation (solid line) for 6H-SiC from G. H. Glover, "Charge multiplication in Au-SiC (6H) Schottky junctions", Journal of Applied Physics, vol. 46, pp. 4842, 1975 [36].

in diameter was used in the center of the diode to avoid the errors in measurement due to the unknown magnitude of the electric field at the edges. A p-type Schottky diode structure with argon ion implant edge termination was used to obtain nearly ideal breakdown voltage. Electron Beam Induced Current (EBIC) technique was used to identify the location of electrically active defects, because defects are known to severely affect the breakdown characteristics of devices. To extract the $\alpha$ from the measured multiplication rates, a thin drift region with a low doping density and a constant electric field profile with depth was used. Raghunathan et al. used the equation $\alpha_{(p)}$=ln$M_p$/W to extract the impact ionization data from the I-V curve obtained by using a special setup of scanning electron microscopy.

Konstantinov et al. reported the first epitaxial 4H SiC diodes with uniform avalanche multiplication and breakdown [38]. Electron and hole ionization rates were measured using the photomultiplication technique, which is a UV He-Cd laser. p+-n-n+ diodes were processed to form positive angle beveled mesa diodes with an angle of about 45° to have a lower electric field at the device periphery than in the bulk. Konstantinov et al. observed that the photocurrent increases by three to four orders of magnitude for the voltage range between $V_b/2$ - $V_b$ and concluded that the increase is due to avalanche multiplication. Konstantinov et al. defined the multiplication coefficient as M=$f_n M_n$+$f_p M_p$, $M_n$ and $M_p$ being the coefficients of electron and hole fractions of the initial photocurrent. Due to the dominant initial current by the generated holes coming from the n region, the multiplication coefficient was defined as M=$M_p$. The coefficient given by the ionization integral is:

$$1 - \frac{1}{M_p} = \int_W^0 \beta * (exp(\int_x^W -(\beta - \alpha)\, dx'))\, dx \tag{2.7}$$

The p-n junction position is at x=W. Extraction of ionization coefficients from photomultiplication data was done by fitting simulated M(V) dependencies to experimental curves. The impact ionization coefficient data from the measurements are shown in Figure 2.5.

Raghunathan and Baliga reported the role of defects on the impact ionization coefficient measurements [39]. Electron beam induced current (EBIC) technique was employed in order to understand the role of defects on breakdown characteristics of SiC. EBIC images revealed that certain defects caused enhanced multiplication that leads to catastrophic failures in SiC diodes. The impact ionization coefficients for holes $\alpha_p$ measured at the defect free site were found to be higher than those measured at a non-defective site. Raghunathan and Baliga also measured that $\alpha_p$ at the defective site was found to be increasing with the increasing temperature. However $\alpha_p$ decreases with increasing temperature in the bulk.

Hatakeyama et al. presented the extracted impact ionization coefficients of p+-n diodes on (0001) and (1120) 4H-SiC epitaxial wafers from avalanche breakdown voltages and the multiplication of a reverse leakage current [40]. Photomultiplication factors were calculated

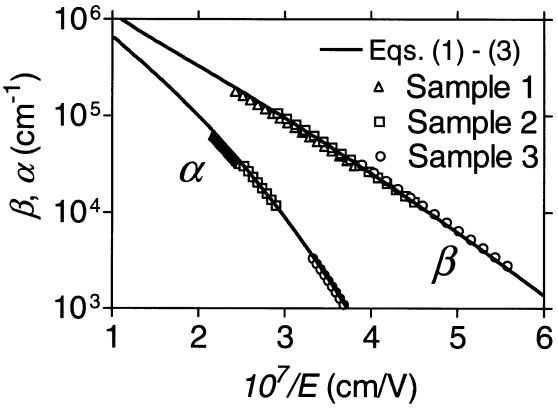


Figure 2.5: Impact Ionization rates for electrons and holes in 4H SiC from A. O. Konstantinov, "Study of Avalanche Breakdown and Impact Ionization in 4H Silicon Carbide", Journal of Electronic Materials, vol. 27, pp. 335, 1998 [38].

from the reverse leakage current versus voltage characteristics under the illumination of UV light using an Ar laser. The results showed that the breakdown voltage of a p+-n diode on a (1120) wafer is 50%-60% of that on a (0001) wafer. It is also measured that the multiplication factor of a p+-n diode on (1120) is smaller than that of a (0001). Hatakeyama et al. obtained the impact ionization data by the fitting procedure of the multiplication versus voltage characteristics and breakdown voltage versus doping density curve.

Loh et al. presented a measurement technique to accurately determine the impact ionization coefficients over a wider electric field range [41]. Both dc and and ac photomultiplication measurements with 244 and 325 nm UV light was performed. Figure 2.6 and 2.7 shows a comparison of ionization coefficients for SiC obtained from Konstantinov et al. [38], Raghunathan and Baliga [39], Hatakeyama et al. [40] and Loh et al. [41].

### 2.2.3 Measurement of Impact Ionization Coefficients in GaN

Gallium Nitride (GaN) is currently a strong research area with its potential for use as a Radio Frequency (RF) and power device due to high breakdown voltage and thermal capacity. As explained in sections A and B, impact ionization coefficients have been measured for Silicon and Silicon Carbide. However, they have not been accurately measured for GaN.

a)Theoretical Studies on I.I. Coefficients in GaN

Kolnik et. al. presented the first calculation of electron initiated impact ionization in bulk zinc-blende and wurtzite phase GaN by using Monte Carlo simulations [11]. At higher fields, 3 MV/cm, they reported the ionization coefficient as 5x10$^4$ cm$^{-1}$ for zinc-blende GaN. The

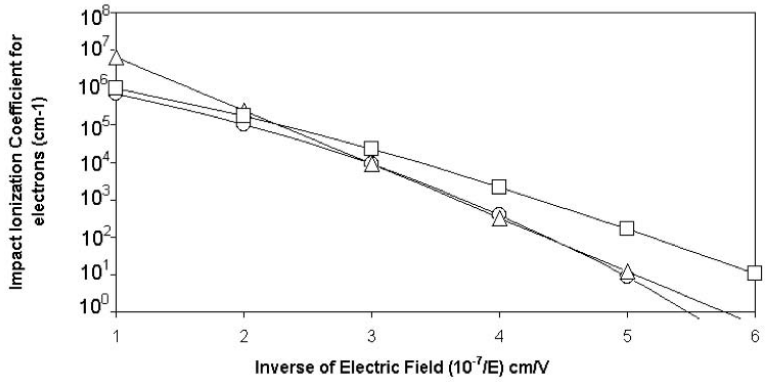


Figure 2.6: SiC Impact Ionization Coefficient for electrons from A. O. Konstantinov et. al., "Study of Avalanche Breakdown and Impact Ionization in 4H Silicon Carbide", Journal of Electronic Materials, vol. 27, pp. 335, 1998 [38] (∘), T. Hatakeyama et. al.,"Impact Ionization Coefficient of 4H Silicon Carbide", Applied Physics Letters, vol. 85, pp. 1380, 2004 [40] ( △) and W. S. Loh et. al., "Impact Ionization Coefficients in 4H-SiC", IEEE Transactions on Electron Devices, vol. 55, pp.1984, 2008 [41] (□).

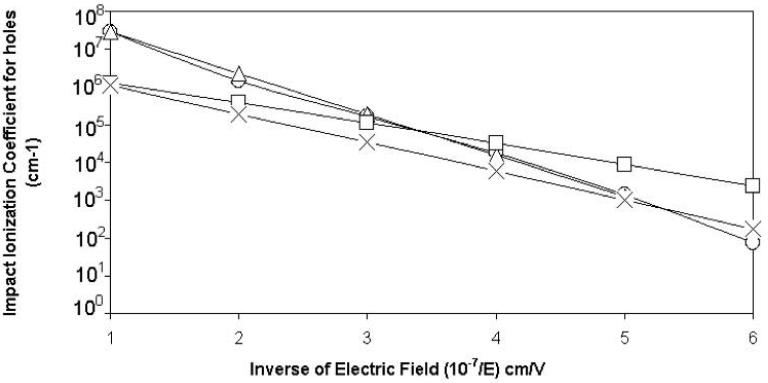


Figure 2.7: SiC Impact Ionization Coefficient for holes from A. O. Konstantinov et. al., "Study of Avalanche Breakdown and Impact Ionization in 4H Silicon Carbide", Journal of Electronic Materials, vol. 27, pp. 335, 1998 [38] (∘), R. Raghunathan and B. J. Baliga, "Role of defects in producing negative temperature dependence of breakdown voltage in SiC", Applied Physics Letters, vol. 72, pp. 3196, 1998 [39] (×) T. Hatakeyama et. al.,"Impact Ionization Coefficient of 4H Silicon Carbide", Applied Physics Letters, vol. 85, pp. 1380, 2004 [40] ( △) and W. S. Loh et. al., "Impact Ionization Coefficients in 4H-SiC", IEEE Transactions on Electron Devices, vol. 55, pp.1984, 2008 [41] (□).

calculated ionization coefficients for wurtzite GaN were more than an order of magnitude lower those for zinc-blende at corresponding fields, due to the higher band gap value of wurtzite.

Oguzman et. al. reported the first theoretical study of hole initiated impact ionization in the zinc-blende and wurtzite phases of GaN by using Monte Carlo simulations [12]. They concluded that the hole impact ionization coefficient is significantly higher in the zinc-blende case than the wurtzite phase, due to the average hole energy being lower in the wurtzite phase than the zinc-blende phase.

Cao et. al. calculated the impact ionization effect in wurtzite phase bulk GaN based on the non-parabolic balance equations [13]. They concluded that impact ionization coefficient changes by a great amount with variations in the scattering rate.

Chen et. al. studied the impact ionization process by using ensembled Monte Carlo (EMC) method [14]. Impact ionization coefficients for both electron and hole were calculated and provided simple equations for them. Bertazzi et. al. also used the Monte Carlo method to calculate the electron and hole impact ionization coefficients along the Γ-A and Γ-M crystallographic directions [15]. Figure 2.8 and 2.9 shows a comparison of ionization coefficients for wurtzite GaN obtained from Kolnik et al.[11], Cao et al.[13], Kunihiro et. al.[16], Chen et. al. [14]and Bertazzi et al [15]. Figure 2.10 shows the impact ionization coefficients for the zinc-blende GaN obtained from Kolnik et. al. [11] and Oguzman et. al [12].

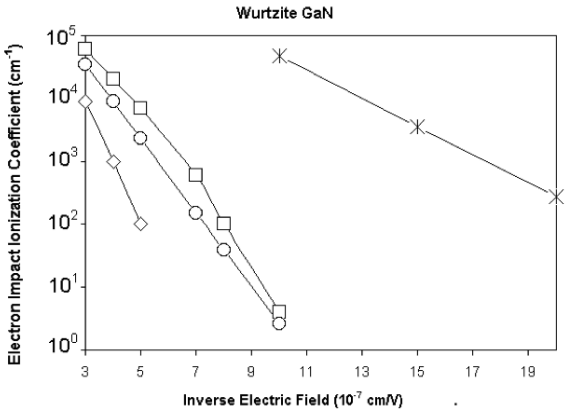


Figure 2.8: Electron Impact Ionization Coefficient for Wurtzite GaN from (□) J. Kolnik et. al., "Monte Carlo calculation of electron initiated impact ionization in bulk zinc-blende and wurtzite GaN", Journal of Applied Physics, vol. 81, 1997 [11], (∘), F. Bertazzi et. al., "Theory of high-field carrier transport and impact ioinization in wurtzite GaN. Part 1: A full band Mote Carlo model", Journal of Applied Physics, vol. 16, 2009 [15], (∗), J. C. Cao and X. L. Lei, "Nonparabolic multivalley balance-equation approach to impact ionization: Application to wurtzite GaN", European Physics Journal, vol. 7, pp. 7983, 1999 [13] and S. Chen and G. Wang, " High-field properties of carrier transport in bulk wurtzite GaN: A Monte Carlo perspective", Journal of Applied Physics, vol. 7, 2008 [14] (◊).

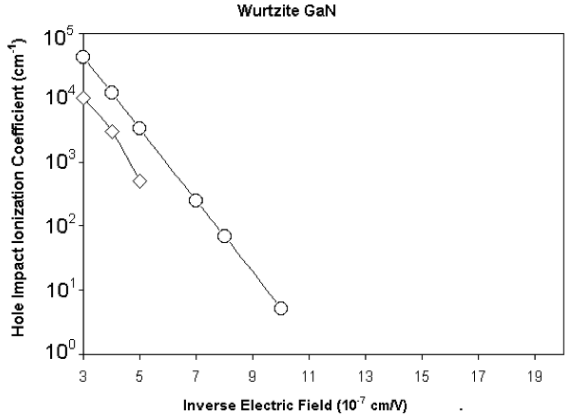


Figure 2.9: Hole Impact Ionization Coefficient for Wurtzite GaN by (∘), F. Bertazzi et. al., "Theory of high-field carrier transport and impact ioinization in wurtzite GaN. Part 1: A full band Mote Carlo model", Journal of Applied Physics, vol. 16, 2009 [15] and S. Chen and G. Wang, " High-field properties of carrier transport in bulk wurtzite GaN: A Monte Carlo perspective", Journal of Applied Physics, vol. 7, 2008 [14] ( ◊).

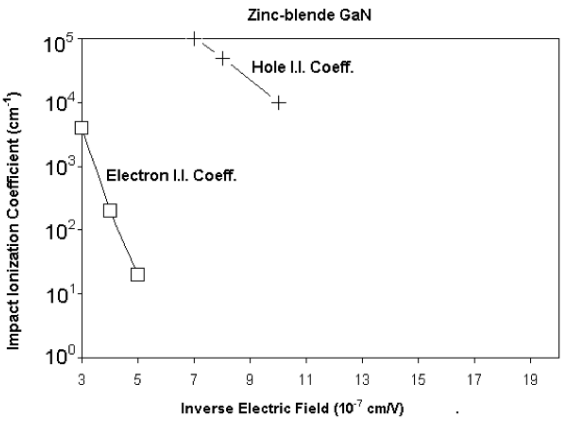


Figure 2.10: Impact Ionization Coefficients for Zinc-blende GaN by (□) J. Kolnik et. al., "Monte Carlo calculation of electron initiated impact ionization in bulk zinc-blende and wurtzite GaN", Journal of Applied Physics, vol. 81, 1997 [11] and (+) I. H. Oguzman et. al., "Theory of hole initiated impact ionization in bulk zincblende and wurtzite GaN", Journal of Applied Physics, vol. 81, 1997 [12].

b)Indirect Measurement of I.I. Coefficients in GaN

Kunihiro et. al. investigated the impact ionization of GaN by electrical characterization of AlGaN/GaN HJFET's with a low gate leakage current and a small gate-drain separation as shown in Figure 2.11 [16]. Gate current (Ig) versus drain voltage (Vd) and drain current (Id) versus drain voltage (Vd) plots obtained from this device are shown in Figure 2.12. The theory for the measurement is the holes generated by the impact ionization along the channel path follows the electric field lines and collected at gate electrode indicated by simulations and the impact ionization coefficients in GaN are evaluated from the gate current in the prebreakdown regime with the method developed by Hui et al.[42]. The number of electron-hole pairs generated by impact ionization is calculated by the product of ionization coefficient $\alpha_n$(E) and the current density $j_n$.

$$I_{hole} = Wx \int_0^{Lg} \int_0^a ((\alpha_n(E) j_n)\, \mathrm{d}x)\, \mathrm{d}y \tag{2.8}$$

where W is the gate width, Lg is the channel length, a is the channel depth, $\alpha_n$(E) is the field-dependent impact ionization coefficient. Since the ionization coefficient is exponentially proportional to the negative inverse of the electric field, Hui et. al. assumed that most of the impact ionization occurs around the region with maximum electric field (Emax) and the equation number 2.8 was approximated as

$$I_{hole} = (\alpha_n(E_{max}) x I_{ds} x I) \tag{2.9}$$

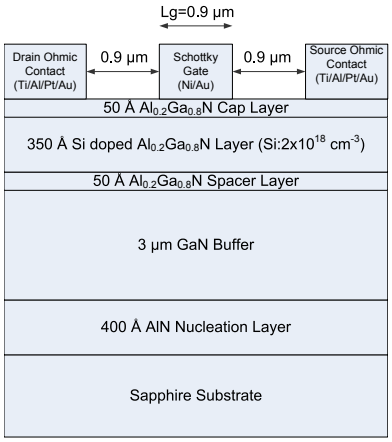


Figure 2.11: Structure of the AlGaN/GaN HJFET from K. Kunihiro et. al., "Experimental Evaluation of Impact Ionization Coeffients in GaN", IEEE Electron Device Letters, vol. 20, 1999 [16].

where $E_{max}$ is approximated as $E_{max}$= $\frac{(V_{ds}-(V_{dsat}))}{Leff}$. Here ($V_{ds}$) is the source-drain voltage, ($V_{dsat}$) is the saturation voltage, which is 4V as shown in Figure 2.12, and Leff is the characteristic length of the high field region. The total gate current was calculated as $I_{hole}$, which is the hole current induced by impact ionization, and the reverse Schottky-gate leakage current $I_{leak}$, $I_{gate}$=$I_{hole}$+$I_{leak}$. It is assumed that the gate current $I_{gate}$ is equal to hole current $I_{hole}$, since the leakage current is much smaller than $I_{hole}$. Then the impact ionization coefficient formula becomes:

$$\alpha_n(E_{max}) = \frac{I_g}{I_{ds} * L_{eff}} \tag{2.10}$$

$I_g$ and $I_{ds}$ were measured as shown in Figure 2.13 and Leff was assumed as 0.4 $\mu$m fitted by Monte Carlo simulations as shown in Figure 2.13. The impact ionization coefficient for electrons in GaN was fitted as 2.9x10$^8 e^{-3.4x10^7/E}$ for electric field region higher than 1x10$^6$ V/cm.

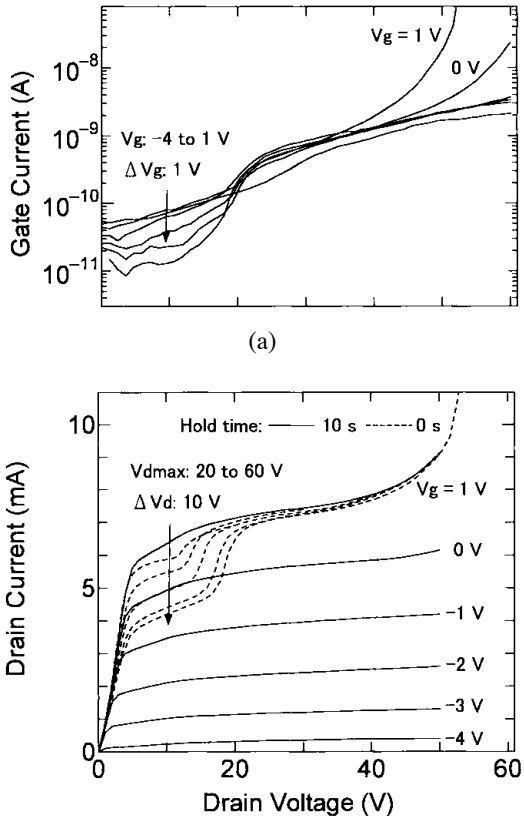


Figure 2.12: DC Characteristics of the AlGaN/GaN HJFET, a)Ig versus Vd, b)Id versus Vd from K. Kunihiro et. al., "Experimental Evaluation of Impact Ionization Coeffients in GaN", IEEE Electron Device Letters, vol. 20, 1999 [16]

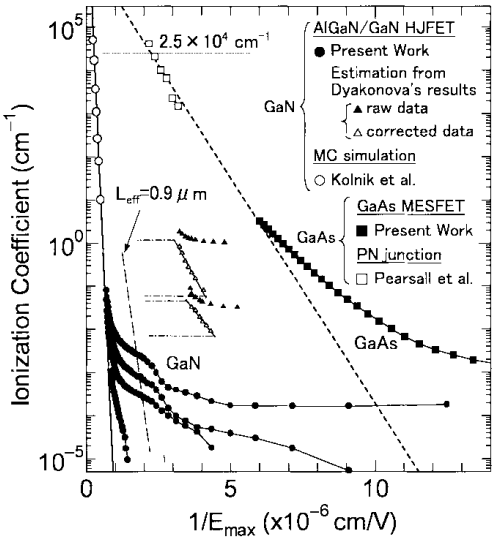


Figure 2.13: Impact Ionization coefficients in GaN extracted from the gate current at Vg=0 V of the AlGaN/GaN HJFET, where Leff=0.4 $\mu$m is assumed from Monte Carlo simulation results from K. Kunihiro et. al., "Experimental Evaluation of Impact Ionization Coeffients in GaN", IEEE Electron Device Letters, vol. 20, 1999 [16].

# Chapter 3

# Methodology

## 3.1 Measurement Methodology

The method used in this work to measure the impact ionization coefficients ($\alpha$) for GaN is based upon the multiplication of carriers generated by a pulsed electron beam in the depletion region of a reverse biased Schottky diode. There are many issues that need to be considered to obtain accurate measurement of impact ionization coefficients in GaN. The first one is the electric field crowding at the edges of the diode that leads to enhanced multiplication of carriers. Since the magnitude of the electric field at the edge is unknown due to uncertain surface charge, any carrier generation near the edges leads to errors in the measurements. To eliminate such errors, measurements were taken at a localized spot at the center of the diodes by using a stationary focused electron beam with a spot size of less than 10 microns. Electric field crowding at the diode edges also results in reducing the breakdown voltage to well below the parallel plane case [43]. This reduces the maximum electric field in the middle of the diode which limits the range over which the impact ionization coefficients can be measured. To avoid this problem, it is crucial to create a good edge termination in the diodes. In this work, a Schottky diode structure with argon ion implant edge termination was used to obtain nearly ideal breakdown voltages [43]. The second problem is the presence of defects in the GaN drift region, which are known to severely affect the breakdown characteristics of devices. Measurements must be made in a defect-free location to extract data representative of the properties of bulk GaN. In this work, the electron beam induced current (EBIC) technique was used to identify the location of electrically active defects and to choose a defect free region for the impact ionization measurements to obtain results representative of defect-free GaN material.

The impact ionization coefficients were extracted from the measured multiplication rates in reversed biased GaN Schottky diodes. A thin drift region with a low doping density is required to obtain a nearly constant electric field profile within the drift region to correlate the

impact ionization coefficients to a particular electric field. Impact ionization coefficients can be extracted from the multiplication data in the case of a constant electric field profile in the drift region by using [44] :

$$1 - \frac{1}{M} = \int_0^W \alpha[exp(\int_0^x -\alpha\, dx)]\, dx. \tag{3.1}$$

where $M$ is the multiplication factor, $\alpha$ is the impact ionization coefficient, and W is the thickness of the drift region. In general, $\alpha$ is a function of electric field (E). However, if the electric field in the depletion region is constant, $\alpha$ becomes independent of x. The above equation then reduces to

$$1 - \frac{1}{M} = \alpha \int_0^W [exp(-\alpha \int_0^x dx)]\, dx. \tag{3.2}$$

which can be further simplified to:

$$1 - \frac{1}{M} = \alpha \int_0^W [exp(-\alpha x)]\, dx. \tag{3.3}$$

Performing the integral yields:

$$1 - \frac{1}{M} = -exp(-\alpha W) + 1 \tag{3.4}$$

Based upon this equation, the impact ionization coefficient can be obtained by using:

$$\alpha = \frac{ln(M)}{W} \tag{3.5}$$

## 3.2 Validation of the Extraction Procedure

Numerical simulations were performed using the Synopsys-TCAD simulator to validate the experimental methodology for the extraction of the impact ionization coefficients and to determine the necessary structures for the test devices. The device structure used for the simulations is shown in Figure 3.1. It consists of a Schottky barrier diode formed on a thin, lightly doped, GaN drift region. The excitation of hole-electron pairs by the electron beam was modeled by adding a photo generation term in the simulation. Simulations were performed to obtain the reverse current-voltage characteristics of the diode with and without the impact ionization models. The impact ionization coefficient models used in the simulator were taken from reference [16] for electrons and reference [12] for holes. The multiplication factor M at each reverse bias value was calculated by taking the ratio of the reverse current obtained with and without the impact ionization. The impact ionization coefficient was then calculated from the

multiplication factor M by using Eq.(3.5). The corresponding electric field was calculated by dividing the reverse bias voltage with the thickness of the epitaxial layer. This approximation is valid, as shown by the electric field profile in Figure 3.2, due to the low ($10^{14}$ $cm^{-3}$) doping concentration of the drift region. The impact ionization coefficients obtained using this procedure were then compared with the values used in the simulation program to determine validity of the methodology.

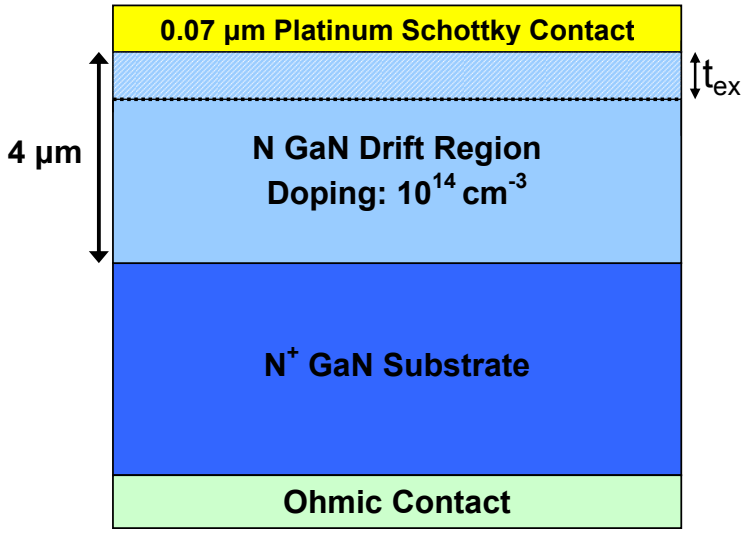


Figure 3.1: Device structure used for numerical simulations

It was found that the impact ionization coefficients for holes and electrons could be separately extracted using the same GaN Schottky diode structure by changing the depth ($t_{ex}$) of the excitation within the drift region. This is demonstrated in Figure 3.3 and Figure 3.4. When the excitation is confined close to the Schottky contact, the extracted value of $\alpha$ fits very well with the value of $\alpha_n$ used during the simulations over a wide range of electric fields as shown in Figure 3.3 in spite of the much larger value for $\alpha_p$. In contrast to this, the extracted value of $\alpha$ fits very well with the value of $\alpha_p$ used during the simulations over a wide range of electric fields as shown in Figure 3.4 when the excitation is performed throughout the drift region.

The effect of changing the excitation thickness ($t_{ex}$) within the drift region on the extracted impact ionization coefficient values is shown in Figure 3.5. From Figure 3.5, it can be observed that $\alpha_n$ can be extracted using methodology when the excitation thickness is less than 0.05 $\mu$m. On the other hand, $\alpha_p$ can be extracted using methodology when the excitation thickness is made larger than 0.3$\mu$m. Neither $\alpha_n$ nor $\alpha_p$ is extracted if the excitation thickness falls between

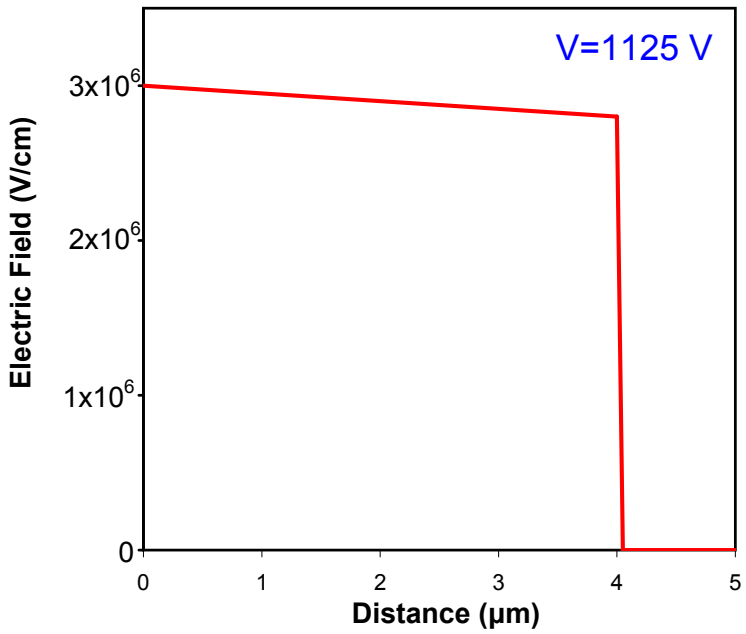


Figure 3.2: The electric field profile obtained from simulations showing that a nearly constant electric field occurs in the drift region

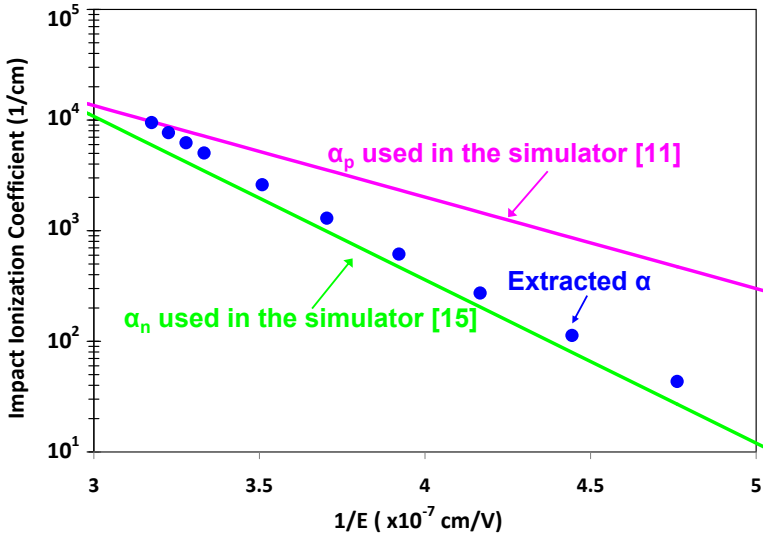


Figure 3.3: Extraction of $\alpha_n$ is possible by using excitation confined near the Schottky contact($t_{ex}$=0.05 $\mu$m).

these values. This can be seen more clearly in Figure 3.6 where the extracted impact ionization coefficient is shown as a function of the excitation thickness for an electric field value of 2x10$^6$

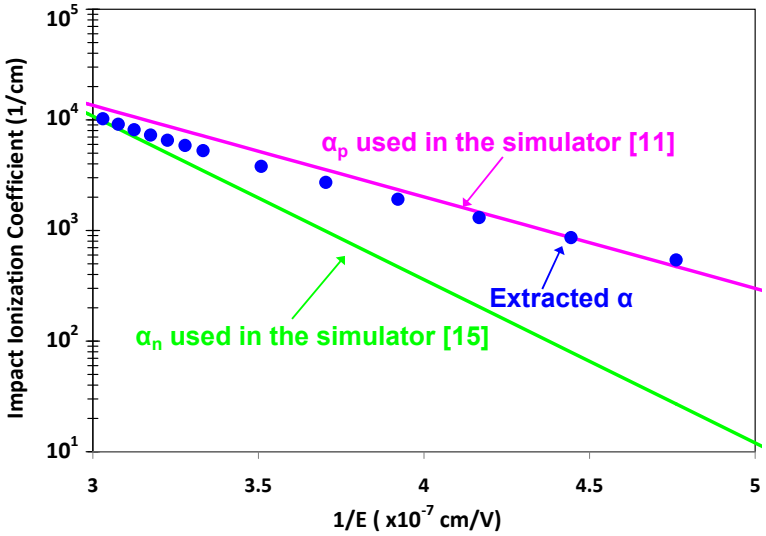


Figure 3.4: Extraction of $\alpha_p$ is possible by excitation throughout the drift region of the Schottky diode($t_{ex}$=4 $\mu$m).

V/cm. From these simulation results, it can be concluded that an excitation thickness of less than 0.05$\mu$m is required to extract $\alpha_n$ and an excitation thickness of greater than 0.3$\mu$m inside the GaN drift region is required to extract $\alpha_p$. This provides the important information required for determination of the electron beam energy utilized during the experimental extraction of the impact ionization coefficients.

## 3.3 Electron Beam Penetration Depth

Calculations were performed to determine the electron beam penetration depth for the device structure shown in Figure 3.1. The penetration depth formula [45]:

$$R_E = 4.28x10^6 E^{1.75/\rho}(cm) \tag{3.6}$$

was used for calculations, where $\rho$ is the sample density (g/$cm^3$)and E the electron energy (keV).

The penetration depth calculation was done for the case of pure GaN, pure Pt and 0.07$\mu$m Pt on GaN. The penetration depth is shown in Figure 3.7 as a function of electron beam energy (keV). Based upon the previous section, an electron beam penetration depth under the Schottky contact of less than 0.05$\mu$m is required to extract $\alpha_n$. From Figure 3.7, it can be concluded that an electron beam energy of 7 keV will penetrate through the Pt contact and produce excitation to a depth of 0.02$\mu$m below the Schottky contact allowing extraction of $\alpha_n$. From Figure 3.7, it

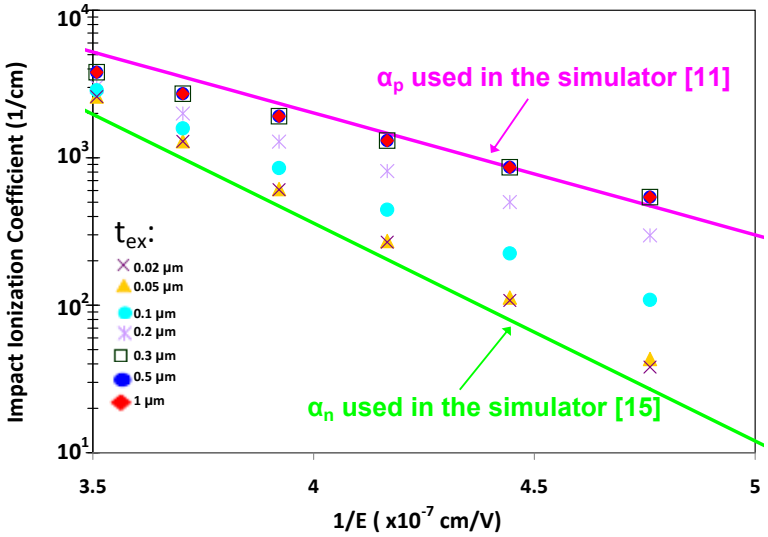


Figure 3.5: Effect of excitation thickness on the extracted impact ionization coefficients. The symbols show the extracted values for the impact ionization coefficients.

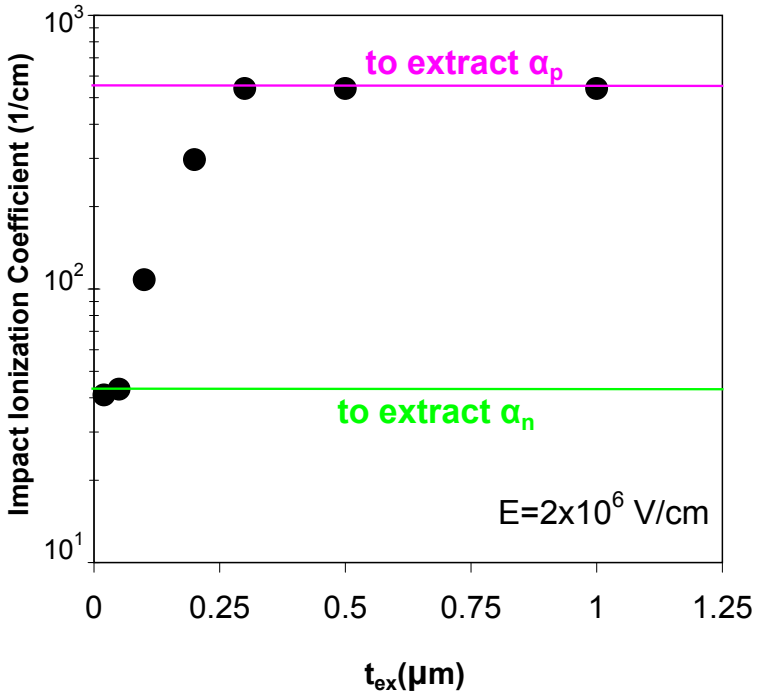


Figure 3.6: Impact of excitation thickness on the extracted impact ionization coefficients for an electric field of $2 \times 10^6$ V/cm in the drift region.

can also be concluded that an electron beam energy of 13keV will produce a penetration depth of 0.3$\mu$m in the GaN under the Schottky contact which is required to extract $\alpha_p$ based upon the analysis in the previous section.

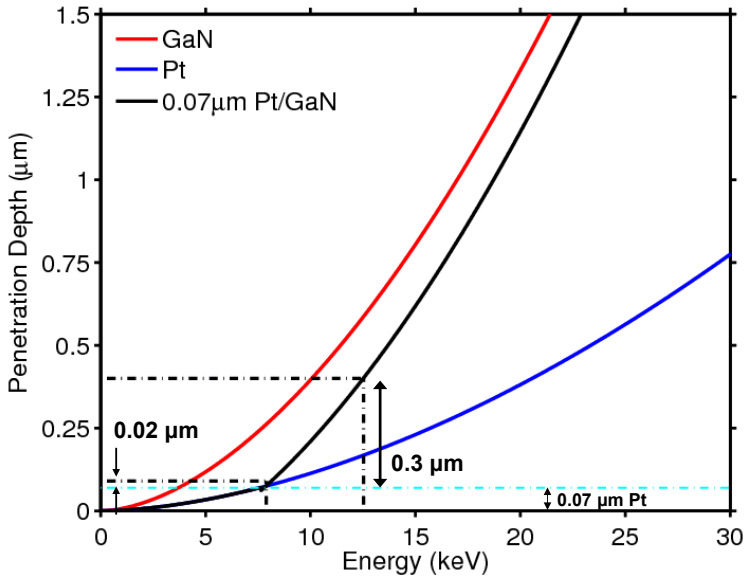


Figure 3.7: Penetration Depth versus Electron Beam Energy

# Chapter 4

# Edge Termination of GaN Devices

Gallium Nitride (GaN) is currently a strong research area with its potential for use for radio frequency (RF) and power devices due to high breakdown field strength and thermal capacity [46]. The critical electric field of GaN (3MV/cm) has been estimated to be more than 10 times greater than that of silicon [47]. This large critical electric field of GaN makes it a promising semiconductor for high voltage applications. In the case of high voltage devices, edge termination plays an extremely crucial role in determining the breakdown voltage [48]. The lack of good edge termination reduces the breakdown voltage of devices to below the ideal limit due to field crowding at the edges as reported for GaN Schottky barrier diodes [47]. In order to be able to obtain the best device performance, the electric field crowding at the edges has to be minimized. Many edge termination methods have been employed for GaN devices for avoiding breakdown by including guard rings, field plates and extension of the contact over an $SiO_2$ layer to reduce field crowding[47][48][49][50][51]. With these edge terminations, it was found that the breakdown voltage was still well below the parallel-plane (ideal) breakdown voltage. A novel planar edge termination technique was demonstrated for Silicon Carbide devices with which nearly ideal plane parallel breakdown voltages can be achieved by creating a thin layer at the edge of the device by using argon ion-implantation [52][53]. In this chapter, this technique is demonstrated to also produce nearly ideal parallel-plane breakdown voltages in GaN Schottky rectifiers.

## 4.1 Planar, Nearly Ideal Edge Termination Technique for GaN Devices

### 4.1.1 Fabrication

Platinum Schottky barrier diodes were fabricated on 4 $\mu$m n-type GaN grown on a bulk GaN wafer with a 2 $\mu$m n+GaN buffer layer. Platinum Schottky barrier diodes have been reported to have good forward and switching characteristics [54][55]. Prior to fabrication of Schottky barrier diodes, the wafers were cleaned in Trichloroethylene (TCE) (5 min.), Acetone (5 min.), Methanol (5 min.) and HCl:H2O (1:1), 5 min., followed by DI water flushing/N2 blow dry. After cleaning, Ti(20nm)/Al(200nm)/Ni(50nm)/Au(50nm) stacked layer was deposited by E-beam evaporation on the backside of the wafer to achieve an ohmic contact. The contact was annealed at 750 °C in $N_2$ for 30 second by RTA. Circular Platinum Schottky contacts (150$\mu$m diameter) with thickness of 1000$\AA$ were deposited by DC magnetron sputtering using a shadow mask on the front side. A cross-section of the fabricated GaN Schottky barrier diodes is shown in Figure 4.1.a with a photomicrograph shown in Figure 4.1.b.

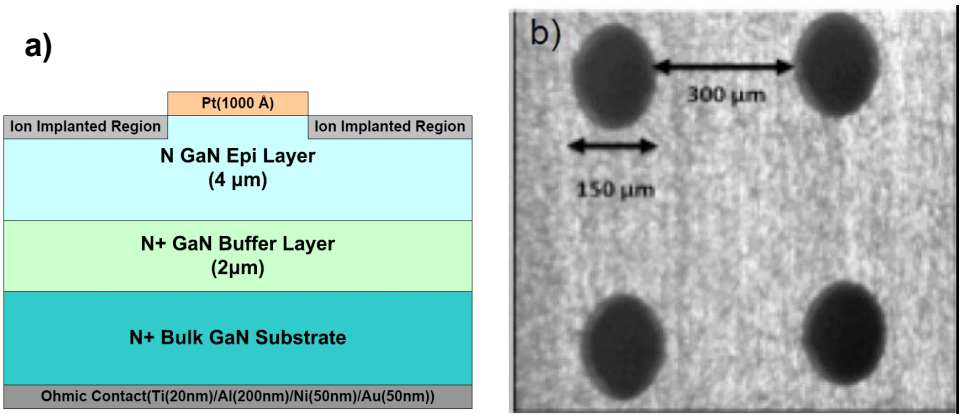


Figure 4.1: a)Structure of the fabricated diode, b) Structure of the shadow mask.

During this work, the edge termination was created using high dose argon implantation. High dose argon implantation is expected to create defects some of which are expected to be located near the mid-gap of GaN. This creates a high resistivity layer at the diode edges which promotes the spreading of the potential along the surface resulting in reduced edge electric field. Unmasked argon implantation was done utilizing the Schottky contact metal to stop the implant damage in the main device area (underneath the Schottky contact). The implant energy was chosen so that the ions were completely stopped by the Pt metal layer to avoid any

degradation of the on-state characteristics of the Schottky barrier diodes. The implant depth in GaN was found to be 309 A for 50keV implantation energy and 444A for 75keV implantation energy from Trim simulations. For Platinum, the implant penetration was found to be 500A for 50keV energy and 750A for 75keV energy demonstrating that the Pt thickness (1000 $\mathring{A}$) is sufficient to mask the argon implants. The dose of argon implantation was increased in steps .

### 4.1.2 Electrical Characterization

The characteristics of the unterminated Schottky barrier diodes were evaluated in both the forward and reverse bias directions. Current-voltage (I-V), capacitance-voltage (C-V) and breakdown voltage measurements were performed. Current-voltage (I-V) measurements were done using a Keithley model 4200 semiconductor characterization system. Prior to IV measurements, the doping concentration of the n-type epitaxial layer was measured using capacitance voltage (CV) analysis. The doping of the n-type epitaxial layer was found to vary between 9x$10^{13}$ $cm^{-3}$and 3x$10^{14}$ $cm^{-3}$ with an average value of 1x$10^{14}$ $cm^{-3}$. Doping concentration versus depth profile for a typical Schottky diode is shown in Figure 4.2. The breakdown voltages were measured for large number of diodes and the the average breakdown voltage of the unterminated Schottky diodes was found as 300 V. The reverse I-V characteristics of all the diodes were measured after each argon ion implantation step. From the forward characteristics, the on-resistance of the diodes were found to be less than 12K$\Omega$-cm$^2$.

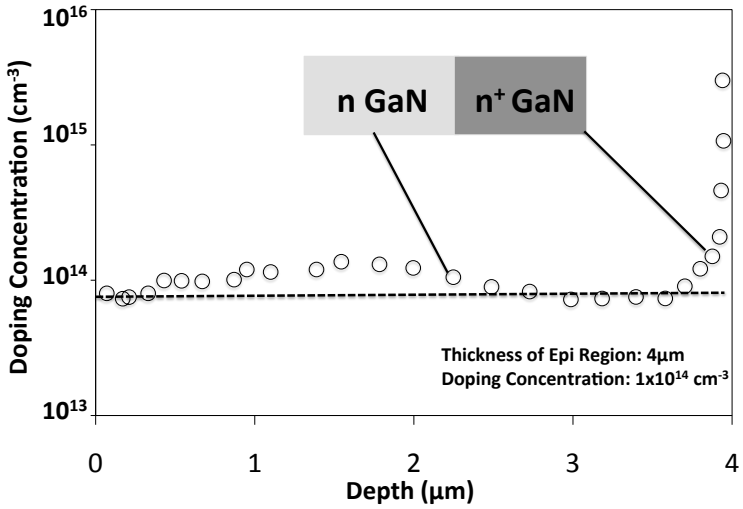


Figure 4.2: Carrier Density($cm^{-3}$) vs. W profile

### 4.1.3 Results and Discussion

To study the effect of the termination on the breakdown voltage of the GaN Schottky barrier diodes, reverse IV measurements were performed. The breakdown voltages of unterminated Schottky barrier diodes were measured for large number of diodes.The unterminated Schottky barrier diodes had the smallest breakdown voltage (300 V±40V ). The breakdown voltage increased to 1500V±100 with implant dose of 2x$10^{16}$ $cm^{-2}$. The breakdown voltage increased from 300V for the unterminated diode to 1600V for the terminated diode as shown in Figure 4.3. The leakage current of the terminated diode is larger at reverse bias voltages below 200V due to contribution from the implanted zone as also reported in SiC devices [52]. The breakdown voltage progressively improved with increase in the implant dose as shown in Figure 4.4. This data demonstrates that an argon implantation dose of 2x$10^{16}$ $cm^{-2}$ is required to obtain close to the parallel-plane breakdown voltage for GaN devices. This dose is 20 times larger than that required for SiC [52]. Forward I-V measurements were also performed and found to be unchanged indicating that the implant had no effect on the on-state characteristics of the diode as shown in Figure 4.5.

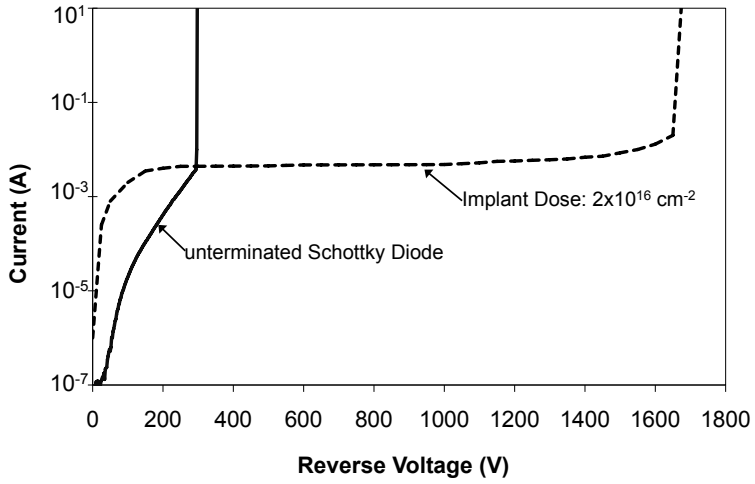


Figure 4.3: Breakdown voltage measurements for a)unterminated Schottky diode and b)Implant Dose:2x$10^{16}$ $cm^{-3}$

The relation between the breakdown voltage and the critical electric field $E_C$ for a punch-through structure is given by [2]:

$$V_{BR} = E_C W - \frac{qN_D W^2}{2\epsilon_S}, \tag{4.1}$$

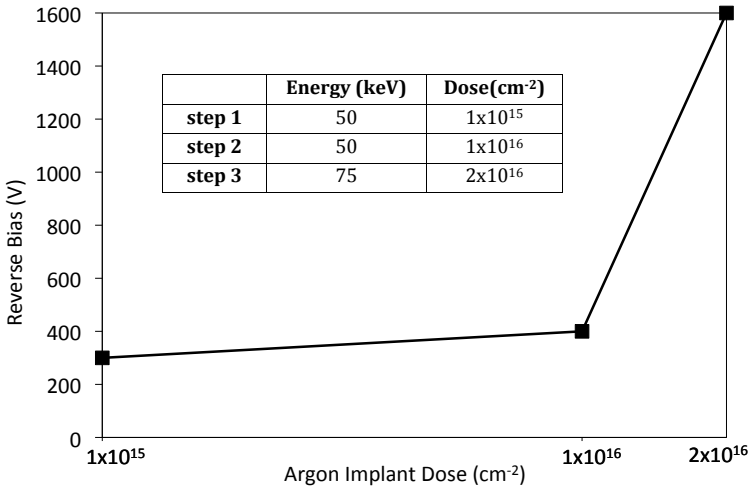


Figure 4.4: Breakdown voltage shown as the function of implant dose on the edges of Schottky barrier diodes.

Table 4.1: Comparison of BFOM for GaN with Silicon and Silicon Carbide

| | Si[2] | SiC [2] | GaN |
|---|---|---|---|
| $\epsilon_r$ | 11.7 | 9.7 | 8.9 |
| $\mu_n$ | 1350 | 1100 | 1000 |
| $E_C$ | 2x10$^5$ | 2x10$^6$ | 3.75x10$^6$ |
| $\epsilon_S \mu_n {E_C}^3$ | 1.12x10$^7$ | 7.56x10$^9$ | 4.16x10$^{10}$ |
| BFOM | 1 | 675 | 3713 |

where $E_C$ is the critical electric field, W is the n GaN layer thickness, q is the electron charge, $\epsilon_S$ is the semiconductor permittivity, and $N_D$ is the residual carrier concentration of the n GaN layer. Using the measured breakdown voltage of 1500 V for the device with n-GaN layer thickness of 4 microns, the critical electric field ($E_C$) is calculated to be 3.75MV/cm. This value is significantly larger than the critical electric field of 3MV/cm assumed for GaN in the literature [47]. Using this large critical electric field, the Baliga's Figure of merit ($\epsilon_S \mu_n {E_C}^3$) is found to be 3713, which is 8.5 times larger than that for SiC (see Table 4.1).

## 4.2 Finite Zone Argon Implant Edge Termination for High Voltage GaN Schottky Rectifiers

In the previous section, a planar edge termination technique with which nearly ideal plane parallel breakdown voltages can be achieved for GaN Schottky barrier diodes with an unmasked argon implant [43] has been proposed and experimentally demonstrated. In this technique, a

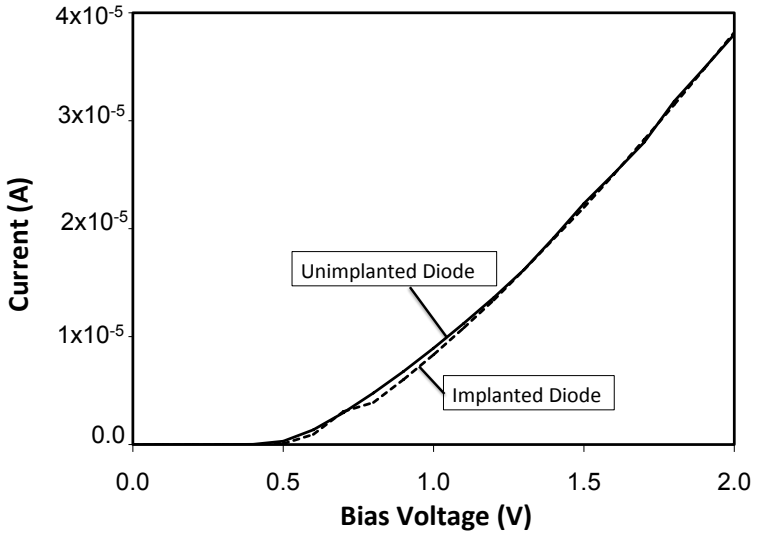


Figure 4.5: Forward IV characteristics for a)unimplanted Schottky diode and b)implanted Schottky diode.

thin amorphous layer was created at the edge of the device by using an argon implantation dose of 2x10$^{16}$ cm$^{-2}$. This high resistivity layer promotes the spreading of the potential along the surface which results in reduced edge electric field under application of a reverse bias voltage. However, an unmasked argon ion implant edge termination would extend to the edges of the GaN chips. For practical devices, a finite edge termination zone is essential. A smaller edge termination zone also contributes less leakage current to the power device. Therefore, it is desirable that the argon implant edge terminated occupies a small and finite area at the periphery of the device. In this section, the minimum implant length required at the periphery of the GaN device to obtain ideal plane parallel breakdown voltage is determined for the first time.

### 4.2.1 Fabrication

Nickel Schottky barrier diodes were fabricated on 4$\mu$m thick, n-type GaN epitaxial layers with a doping of 4x10$^{14}$ cm$^{-3}$ grown on a sapphire substrate wafer with a 2 $\mu$m thick, n$^{+}$-GaN buffer layer. Prior to fabrication of Schottky barrier diodes, the wafer was cleaned by Trichloroethylene (TCE) (5 min.), Acetone (5 min.), Methanol (5 min.) and HCl:H2O (1:1), 5 min., followed by DI water flushing/N2 blow dry. Circular (150$\mu$m diameter) Schottky barrier diodes were fabricated by evaporation of 1000$\mathring{A}$ of Nickel on top of the GaN epitaxial layer. To obtain a finite edge termination region, GaN Schottky barrier diodes were terminated with the implantation restricted to a finite distance around periphery by masking the argon ion

implantation using a 1.5 $\mu$m thick photoresist mask alligned to the metal layer. After defining the finite zones by using photoresist, argon implantation with a tilt angle of 7 degree was done with an implant dose and energy of 2x$10^{16}$ $cm^{-2}$ and 50 keV, respectively. The implant dose and energy was based upon the results obtained from the previously reported work [43]. The cross section of the terminated structure is shown in Figure 4.6. The edge of the argon implanted region was self aligned to the Schottky metal because the argon implant can not penetrate the 1000$\mathring{A}$ of Nickel. The length of the implanted region in the lateral direction ($L_{ET}$) was varied from 5 to 200 $\mu$m.

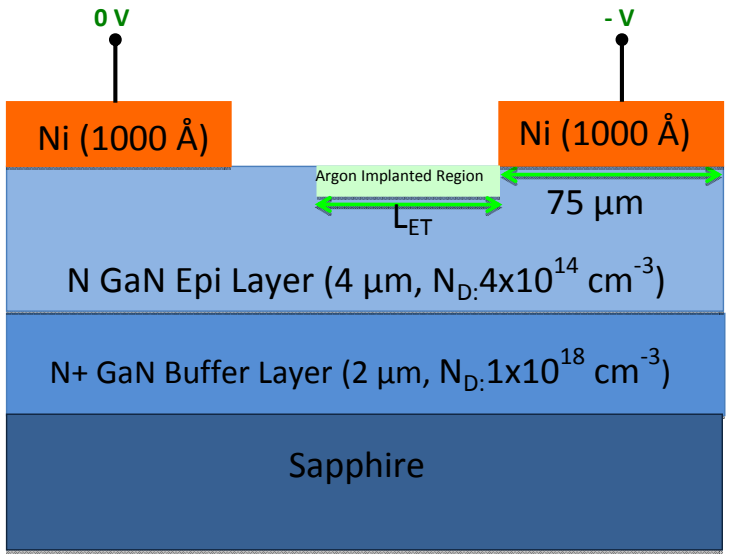


Figure 4.6: Cross section of the fabricated GaN Schottky barrier diodes.

### 4.2.2 Results and Discussion

Back-to-back Schottky diodes were used for measurements due to the complexity of the Ohmic contact fabrication and the related processes, such as mesa etching, ohmic contact lithography, surface preparation, and formation annealing. During measurement of reverse I-V characteristics of back-to-back Schottky diodes, one diode is forward biased with a low voltage across it while the second diode is reverse biased as shown in the Figure 4.7. Under high reverse bias voltage, most of the potential drop occurs on the reverse biased Schottky contact where the depletion region extends as shown in Figure 4.7. At high reverse biases, the lightly doped GaN epi-region is completely depleted and all the potential drop is inside this depletion region

where E-field looks like the GaN-on-GaN devices.

The reverse I-V characteristics of the terminated structures with various implant lengths in the lateral direction are shown in Figure 4.8. As expected, the breakdown voltage increases with increasing implant length. However, the breakdown voltage improvement was not significant above an edge termination length of 50 $\mu$m. Breakdown voltages as high as 1700 V were measured for the terminated diode which is close to the ideal plane parallel voltage and about 4 times higher than that of the unterminated diodes. Figure 4.9 shows the breakdown voltage as a function of implant length ($L_{ET}$). This graph demonstrates that a 50 $\mu$m edge termination length is adequate to yield the nearly ideal breakdown voltage.

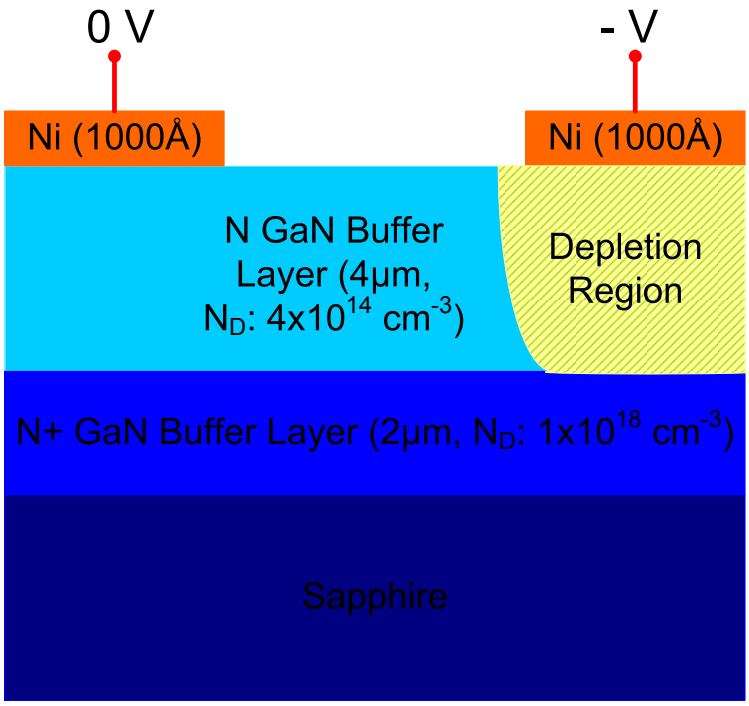


Figure 4.7: Back-to-back Schottky diode

The plot of leakage current as a function of implant length ($L_{ET}$) in the lateral direction for reverse biases of 350 V and at 80% of breakdown voltage for each implant zone length is shown in Figure 4.10. The leakage current flowing through the GaN Schottky diodes was found to be increase with increasing implant region length ($L_{ET}$) at the periphery. This increase in leakage current indicates that the implanted region at the periphery of the diode contributes a significant leakage current to the Schottky diode.

Numerical simulations were performed using Synopsys-TCAD for GaN Schottky barrier

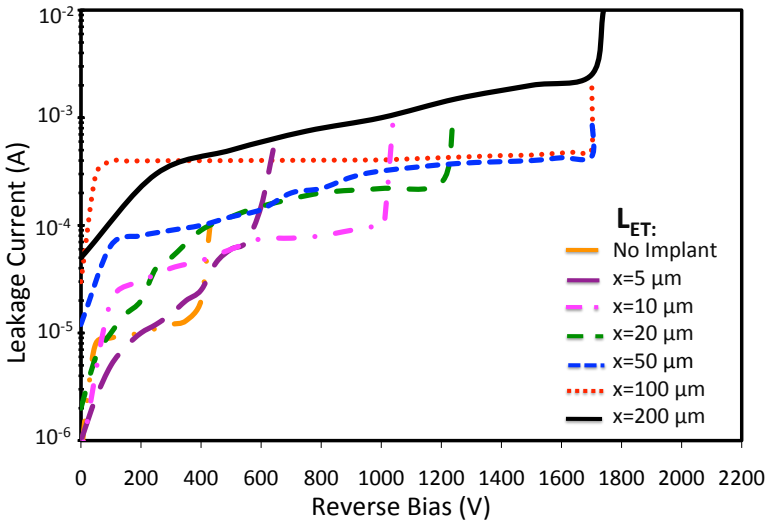


Figure 4.8: Measured reverse current voltage characteristics for terminated GaN Schottky barrier structures with various implant region lengths.

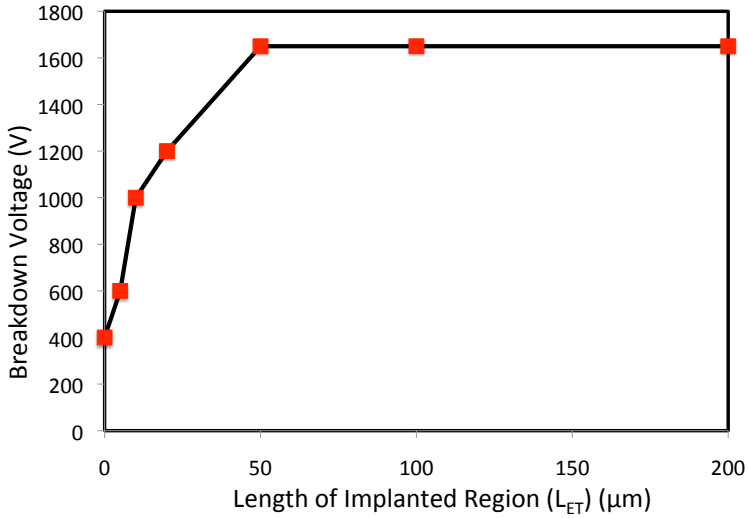


Figure 4.9: Experimental data on dependence of breakdown voltage on edge termination length.

diodes to understand the effect of the length of implant region on breakdown voltage. The cross section of the simulated structure is shown in Figure 4.6. The implanted region at the edge of the Schottky barrier diode was modeled by the addition of single mid-gap acceptor level in the argon implanted region in addition to the dopant level already present in the unimplanted drift region. The plane parallel voltage was found to be 1750 V while the breakdown voltage of the unterminated structure was found to be 420 V. The length of the implanted region was

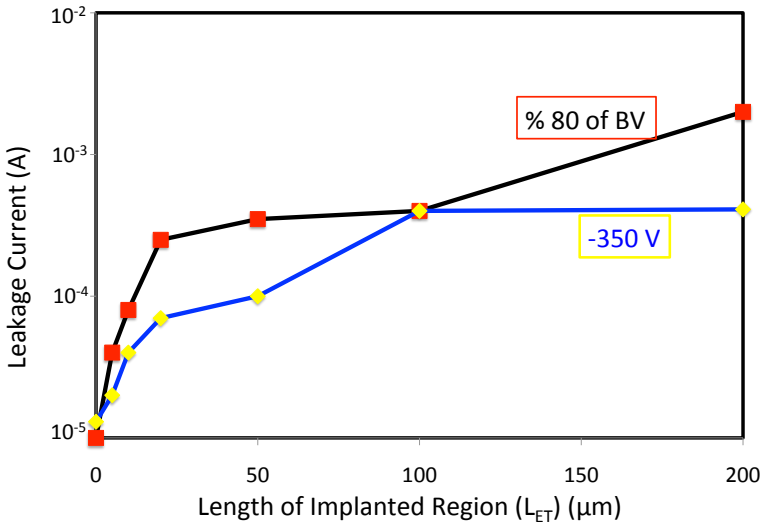


Figure 4.10: Experimental data on increase in leakage current of terminated structure with increasing implant region length.

varied to study its influence on the breakdown voltage and to observe the potential spreading in the lateral direction. Figure 4.11 shows the electric field at the breakdown voltage for implant zone lengths ($L_{ET}$) from 5 $\mu$m to 200 $\mu$m. Note the increased spreading of the electric field along the surface at the edges as the implant zone length increases from 5 $\mu$m to 50 $\mu$m. For 100 $\mu$m and 200 $\mu$m implant lengths, the electric field spreading was observed to be limited to 50 $\mu$m. For all cases, breakdown occurs when the same electric field value is reached at the edge of the Schottky contact.

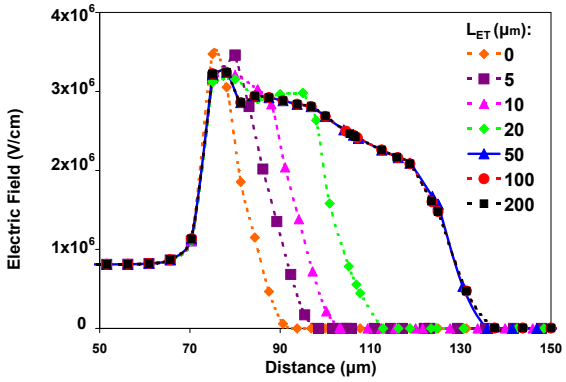


Figure 4.11: Electric Field obtained using Numerical Simulations for terminated structure as a function of implant region length

Figure 4.12 shows the breakdown voltage obtained from numerical simulations for each implant length. The breakdown voltage values obtained from the simulations are in close agreement with the breakdown voltage data measured from fabricated diodes validating the model.

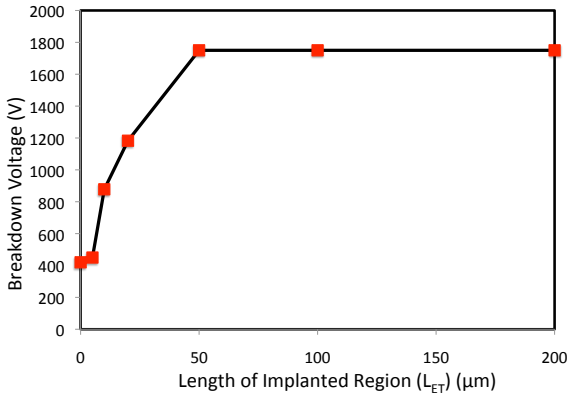


Figure 4.12: Simulation results of breakdown voltage dependence on edge termination length.

Forward conduction behavior of GaN Schottky barrier diodes was performed and found to be the same before and after the argon implanted termination indicating that the implant had no effect on the on-state characteristics of the diode as reported in previous work [43].

The relation between the breakdown voltage and the critical electric field $E_C$ for a punch-through diode is expressed by [2]:

$$V_{BR} = (E_C W) - (qN_D W^2/2\epsilon_S), \tag{4.2}$$

where $E_C$ is the critical electric field, W is the n-GaN layer thickness, q is the electron charge, $\epsilon_S$ is the semiconductor permittivity, and $N_D$ is the doping concentration of the n-GaN layer. Using the measured breakdown voltage of 1700V for the device with an n-GaN layer thickness of 4$\mu$m, the critical electric field ($E_C$) is calculated to be 4.2 MV/cm. This value of critical electric field for breakdown for GaN grown on sapphire substrates is in very close agreement with a critical electric field of 3.75MV/cm found in the previous work for GaN grown on GaN substrates [43].

# Chapter 5

# Electron Beam Induced Current (EBIC) Technique

## 5.1 Scanning electron microscopy

The Scanning Electron Microscope (SEM), a powerful and versatile analytical tool, has proven to be indispensable for characterization of semiconductor devices and materials. An electron gun emits electrons (by thermionic or field emission) which are accelerated down the column by a large potential energy (typically l-30 keV). Electromagnetic lenses and mechanical apertures are used to demagnify and focus the electrons to form an electron probe of small diameter and high current density. The lenses are adjusted to change the focal length of the primary electron beam to focus the image, and to change the electron beam diameter and current density. The ability to change the focal length of the electronic lenses and the size of the apertures allows the microscopist to optimize the spatial resolution and the depth of focus in order to obtained the desired image or signal. The scanning coils deflect the electron beam over the surface of the specimen in a raster pattern. The scanning circuit allows the operator to vary, the size of the area scanned (i e. to change the magnification), and to scan at slow speeds for photographs or at fast speeds for observation purposes. The video display is a Cathode Ray Tube (CRT). There is a video amplifier which synchronizes the raster scan of the SEM cathode ray tube with the raster scan of the electron probe striking the sample. This ensures a one-one correspondence between the signal collected at any particular point on the specimen surface and the brightness of the analogous point on the CRT screen. One important component of the SEM is the specimen stage. The stage of the SEM is adapted to provide heating of the sample. This feature is included to allow us to do impact ionization measurements at temperatures as high as 200°C.

The primary electrons of the electron beam interact with the specimen producing a large

number of detectable signals. Multiple scattering of the incident or primary electrons as they enter the specimen causes them to follow numerous trajectories. The interaction of the electron beam in the semiconductor generates various signals at different depths. Elastic collisions of the primary electrons with atoms in the specimen result in the generation of backscattered electrons. Backscattered electrons are incident electrons that have been scattered back and have energies nearly as high as the incident beam. They can be generated from deep within the specimen and still escape the surface. Inelastic collisions result in gradual loss of the incident electrons until they are absorbed by the specimen. Inelastic collisions results in the generation of various kinds of signals, namely the secondary electrons, Auger electrons, X-rays, and visible and infrared light. Secondary electrons are low energy and therefore escape only when generated close to the surface of the specimen. For these reasons secondary electrons mainly yield information about the surface morphology. Like the backscattered electrons, the x-ray photons can approach the energy of the incident electrons and therefore can be generated over a large volume. In this work, mainly a mode of image formation in which the specimen itself acts as a detector or collector of the electronic charge that make up the video signal has been used. This mode of imaging is called the Electron Beam Induced Current mode (EBIC).

## 5.2 EBIC Technique

In this study, electron beam induced current (EBIC) technique was employed in order to understand the role of defects on the breakdown characteristics of GaN. In these measurements, the electron beam induced current (EBIC) technique was used in a scanning electron microscope (SEM) to first identify the location of electrically active defects. The experimental setup (Fig. 5.1) was established using EBIC that allowed us to apply reverse biases as high as 500 V on these diodes to image sites of enhanced multiplication. The basic principle of operation of the SEM in the EBIC mode is as follows: The electron beam incident in the semiconductor generates carriers. If these carriers were generated in a depletion region of a reverse biased junction, the generated carriers are immediately swept away by the built in electric field of the depletion region and are collected to induce a current in an external circuit called the electron beam induced current. As the electron beam rasters the surface of the specimen, different values of the EBIC signal is generated at different points. If there is an electrically active defect in the depletion region, such as a recombination center or trap, the EBIC current generated at the defective site will be very low due to excess recombination. Therefore, this defect appears as a dark region inside the active device. On the other hand, by increasing the reverse bias, it is possible to image defective sites of enhanced multiplication. Due to enhanced multiplication at the defect site, these defects appear as bright spots in the EBIC image.

Defects occasionally occur in GaN films grown by Metallorganic Chemical Vapor Deposition

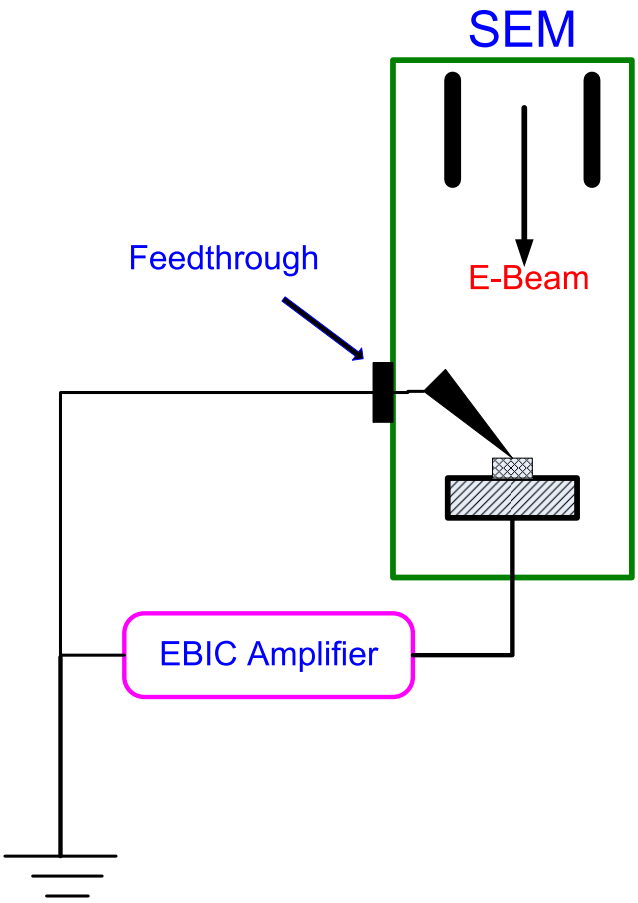


Figure 5.1: Schematic of the experimental setup of EBIC Measurements

(MOCVD) and Hybride Vapor Phase Epitaxy (HVPE) techniques. The frequency of occurrence and density of these defects varies depending on the growth conditions, especially on doping type and level. Defects can be examined by both macroscopic and microscopic ways of luminescence measurement. Macroscopic defects, ranging from some nanometers to several micrometers. Macroscopic defects are mainly twins, inversion domains, hexagonal pits or crevices on the nitrogen face and columnar growth or hillocks on gallium face. These defects can be identified via atomic force microscopy (AFM) and scanning electron microscopy (SEM)[56]. Microscopic defects range from some nanometers to the sub-nm range. Microscopic defects are frequently formed both in Mg-doped and in unintentionally oxygen/carbon doped GaN single crystal, such as small voids, dislocations and strains. These defects can be measured by cathodoluminescence (CL) and micro-photoluminescence (PL) with high spatial resolution [56]. Macroscopic defects are the ones that are detected by the EBIC technique.

For the impact ionization measurements, it was essential to obtain near ideal breakdown in the devices in order to obtain high multiplication in the measured data. Therefore, it is essential to use a good termination technique. Hence there was a need to study the effectiveness of Argon termination technique. EBIC technique has been used to study the effectiveness of the termination technique.

## 5.3 EBIC Study of Edge Termination

EBIC measurements were made on unterminated Schottky diodes and also on diodes with argon ion implant termination for reverse biases up to 100 V to understand the nature of electric field crowding at the edges.

### 5.3.1 Unterminated Diodes

Fig. 5.2 shows the EBIC line scan made across an unterminated GaN Schottky diode. EBIC line scan on these diodes for increasing reverse biases of 50 and 75 V exhibited enhancement of the current localized at the edge of the diode. Based upon this, it has been concluded that there is significant multiplication effect at the edge due to impact ionization arising from a high electric field. This leads to a severe reduction in breakdown voltages of these diodes. Figure 5.3 shows the EBIC image of the GaN Schottky diode at reverse biases of 75 V and 100 V. It can seen that EBIC current increases at the edges as voltage increases. Enhanced multiplication due to defect site is shown in this figure.

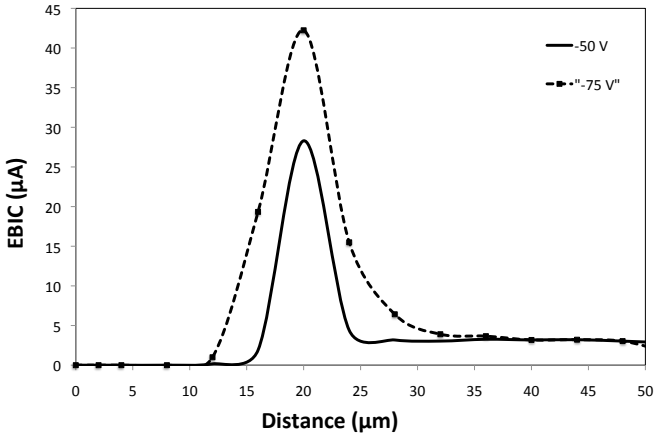


Figure 5.2: EBIC line scan on unterminated GaN Schottky Barrier Diode

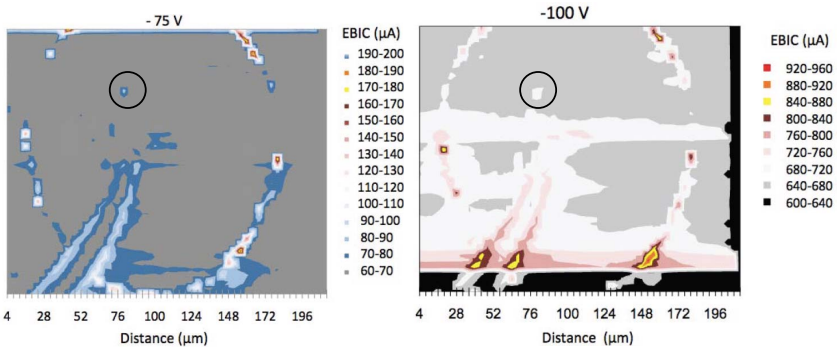


Figure 5.3: EBIC image of an unterminated GaN Schottky diode at a reverse bias of -75V and -100V at room temperature

### 5.3.2 Argon Ion Implant Terminated Diodes

Argon Ion implant termination has been shown to give near ideal breakdown for GaN Schottky diodes [43]. The argon implantation is believed to create a thin high resistance layer at the surface beyond the edges of the diode. This promotes the spreading of the potential along the surface resulting in reduced edge electric field. Fig. 5.4 shows the EBIC data obtained for an argon ion implant terminated diode. It is important to note that there is not a significant increase in the peak value of the EBIC signal at the metal edge. From this, it is concluded that the implanted layer is very effective of reducing the field crowding at the edges by spreading of the depletion edge along the implanted region with increasing reverse biases, while negligible spreading is observed for an unterminated diode. It can be concluded that, this edge termination is effective in improving the breakdown characteristics of the diode.

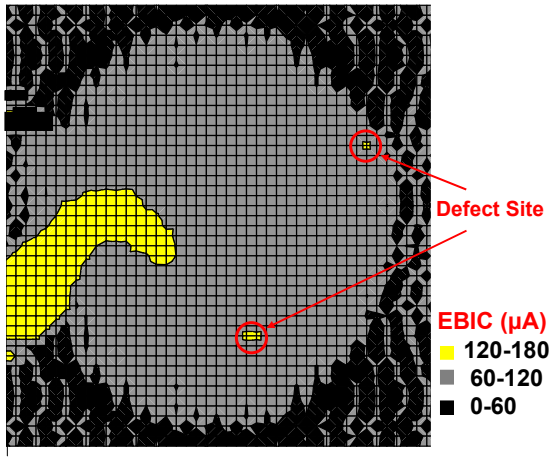


Figure 5.4: EBIC image of a terminated GaN Schottky diode at a reverse bias of 75 V at room temperature.

# Chapter 6

# Measurement of Impact Ionization Coefficients for GaN

In order to obtain a clear understanding of the breakdown characteristics of a power device, it is important to have an exact knowledge of the impact ionization coefficients for electrons and holes in the semiconductor. The impact ionization coefficients not only determine the reverse characteristics of a device but also influence the on-state voltage drop of unipolar devices, such as power MOSFETs and Schottky rectifiers, because the specific on-resistance of the drift region is inversely proportional to the Baliga's figure of merit (BFOM=$\epsilon_s \mu {E_c}^3$) [2], where $\epsilon_s$ is the dielectric constant, $\mu$ is the carrier mobility, and $E_c$ is the critical electric field for breakdown which is determined by the impact ionization coefficients.

Electron and hole impact ionization coefficients in GaN as a function of electric field were first modeled based upon Monte Carlo simulations [11] [12]. Cao et. al. [13] have calculated the impact ionization effect in wurtzite phase bulk GaN based on the non-parabolic balance equation. Chen et. al. [14] studied the impact ionization process by using an ensembled Monte Carlo (EMC) method. Bertazzi et. al. [15] also used the Monte Carlo method to calculate the electron and hole impact ionization coefficients along the Γ-A and Γ-M crystallographic directions. Subsequently, Kunihiro et. al. [16] obtained impact ionization of GaN by electrical characterization of AlGaN/GaN HJFETs grown on sapphire substrates. However, this is an indirect extraction method based upon fitting the electrical characteristics of transistors. McClintock et. al. [17] measured the electron and hole impact ionization coefficients by illuminating GaN avalanche photodiodes grown on sapphire substrates. There are various limitations to this technique. Firstly, there is a high probability that there are defects in the large illumination area which could lead to errors in the measured data. In addition, high electric fields at the illuminated edges of the diodes can enhance the impact ionization producing errors in the extraction procedure.

In this chapter, the measured values for the impact ionization coefficients for electrons and holes are reported for GaN grown on bulk GaN substrates and for GaN grown on Sapphire substrates by using the pulsed electron beam technique to generate carriers within the depletion region of GaN Schottky diodes. This method allows extraction of impact ionization rates in defect free regions of the material by isolating diodes containing defects by using an EBIC image. In addition, the electron beam can be focused away from the edges of the diodes, because it can penetrate the Schottky contact metal layer, to avoid enhanced impact ionization from the larger electric fields at the edges of diodes.

## 6.1 Experimental Setup

A schematic of the experimental measurement setup for the extraction of the impact ionization coefficients is shown in Figure 6.1. Diodes were first imaged using EBIC in order to isolate defect free devices. Impact ionization measurements were then performed on these diodes using the pulsed electron beam set-up. Carriers were generated in the GaN Schottky barrier diode test structure by using the electron beam in a Hitachi S-2700 scanning electron microscope. The electron beam was pulsed using a beam blanking setup to allow using a lock-in amplifier to obtain the multiplication data while rejecting ambient noise. To reject the ambient noise the value of the lock-in amplifier should be set to zero by adjusting the offset during the dark measurement. The pulse generator should be turned on first. Then the beam blanker should be turned-on. Power supply is the next one, but the high power button should be off at first to prevent an unexpected failure. The lock-in amplifier is the last one to turn on to protect it. The beam blanking device consists of two electrodes, placed in the electron gun region, which are used to deflect the beam with an externally applied bias that is produced by a pulse generator. The lock-in amplifier is synchronized to the pulse generator. The lock-in amplifier measures the voltage across the sense resistor ($R_s$ of 1.8k$\Omega$) to obtain the current generated by the pulsed electron beam excitation of the reverse biased GaN Schottky diode. The lock-in amplifier signal can then be used to obtain the multiplication factor (M). The circuit includes a resistor ($R_p$ of 333k$\Omega$) to protect the instruments in case of catastrophic failure of the test diode. The setup was automated using a graphical programming tool (LABVIEW) to allow extensive and accurate data acquisition. The software ramps up the voltage in the power supply at specific steps. For every reverse bias value, impact reads the corresponding generated current value from the Lock-in amplifier. It also reads the value of the bias from the digital multimeter connected across the diode. Since there are going to be voltage drops across the resistances in the circuit, the bias on the power supply need not correspond to the bias across the diode, specially close to the breakdown where the leakage current increases drastically. Then, a plot of the generated current as a function of the reverse bias across the diode was plotted.

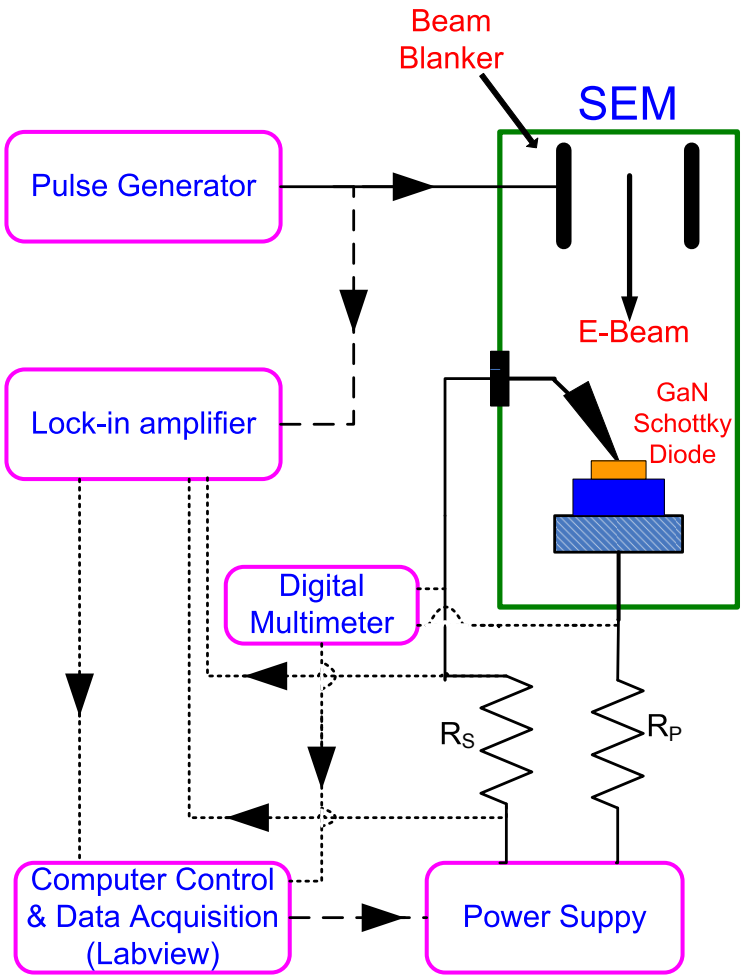


Figure 6.1: Schematic of the experimental setup

The unique capability of the setup is the presence of a specially designed heating stage that will allow us to perform the measurements at higher temperatures. Measurements of impact ionization coefficients at higher temperatures will allow us to predict the variation of breakdown voltage with temperature.

## 6.2 Measurement of Impact Ionization Coefficients for GaN Epilayer Grown on Bulk GaN Substrate

### 6.2.1 Device Fabrication and Characterization

Platinum Schottky barrier diodes were fabricated on a 4$\mu$m thick n-type GaN epitaxial layer grown on top of a 2$\mu$m thick $N^+$ GaN epitaxial buffer layer grown on the $N^+$ GaN substrate to reduce defects in the drift region. Prior to the fabrication of the Schottky barrier diodes, the wafer was cleaned using trichloroethylene (5 min), acetone (5 min), methanol (5 min), and HCl:H2O (1:1) (5 min), followed by DI water flushing/$N_2$ blow drying. After cleaning, an ohmic contact of Ti (20 nm)/Al (200 nm)/Ni (50 nm)/Au (50 nm) was deposited by e-beam evaporation on the backside of the wafer. The ohmic contact was annealed at 750 °C in $N_2$ for 30 s by RTA. Circular Platinum Schottky contacts with 150-$\mu$m diameter and a thickness of 1000 $\mathring{A}$ were deposited on the front side by DC magnetron sputtering using a shadow mask.

As explained in Chapter 4, an argon implant was performed around the edges of the diodes to obtain nearly ideal breakdown voltage [43]. The doping concentration and thickness of the epitaxial layers was obtained using C-V measurement. The doping of the n-type epitaxial layer was found to vary between 9x10$^{13}$ and 3x10$^{14}$ $cm^{-3}$ with an average value of 1x10$^{14}$ $cm^{-3}$. The forward and reverse characteristics of the diode were studied using I-V measurement. The breakdown voltages were measured for a large number of diodes, and the average breakdown voltage of the Schottky diodes was found to be 1500 V after edge termination.

### 6.2.2 Impact Ionization Data

A typical plot of the current-voltage characteristics for a GaN Schottky diode obtained using the pulsed electron beam setup described above with beam energy of 13keV is shown in Figure 6.2. The multiplication factor (M) was obtained by taking the ratio of the measured pulsed electron beam current to the extrapolated i-v curve from lower reverse bias voltages. The extrapolated i-v curve was obtained by a linear fit to the first five data points at low (<10V) reverse bias voltages. This line represents the current without impact ionization due to the small values for the impact ionization coefficients at low reverse bias voltages. The current levels of below 100nA and on resistance below 12K$\Omega$-cm$^2$ yields a negligible voltage drop (less than couple of volts) compared to >1200V breakdown voltage. Therefore the impact of series resistance in measurements can be ignored.

Measurements were performed to show the repeatability of the data by performing the extraction of the impact ionization ten times at the same location in the GaN Schottky diode with a fixed electron beam energy of 7keV. The mean value and the standard deviation are shown in Figure 6.3. The standard deviation increases at lower electric fields due to the re-

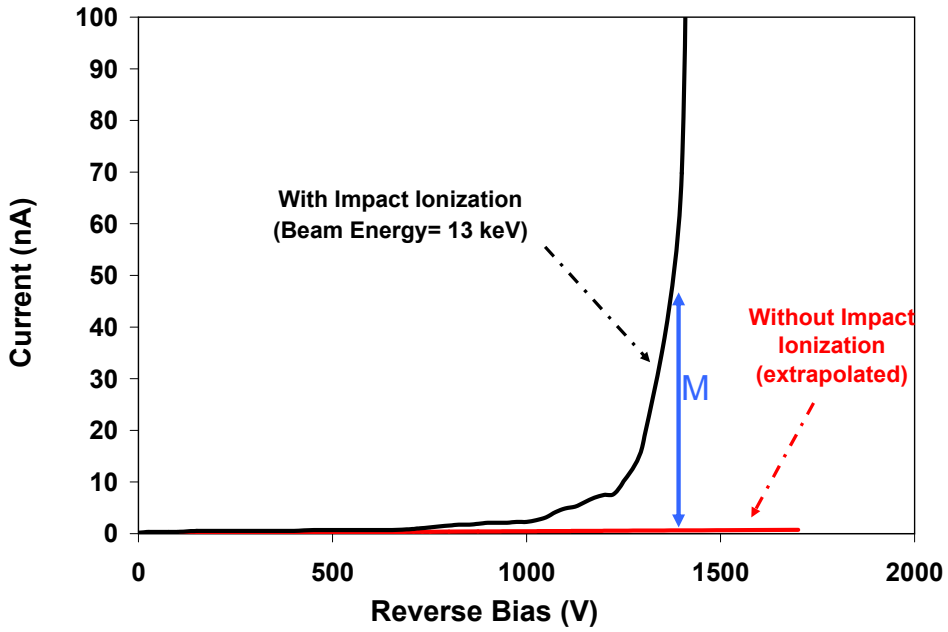


Figure 6.2: Measured multiplication factor with increasing reverse bias on the GaN Schottky diode.

duced multiplication but is very small for high electric field values which are of importance to determination of breakdown in GaN devices.

In chapter 3, it was demonstrated by numerical simulations that the extracted impact ionization values depend on the excitation depth. This was experimentally investigated by varying the electron beam energy. The dependence of the extracted impact ionization data on the electron beam energy is shown in Figure 6.4. It can be observed that the extracted data becomes independent of electron beam energy when it is reduced below 7 keV. This data corresponds to the impact ionization coefficient for electrons as discussed in Chapter 3. From Figure 6.5, it can also be observed that the impact ionization data becomes independent of electron beam energy when it is increased beyond 13keV. This data correspondence to the impact ionization coefficient for holes as discussed in Chapter 3. These results validate the measurement methodology proposed in this paper allowing extraction of the impact ionization coefficients for both electrons and holes using the same diode test structure.

Using the automated setup, extensive measurements of impact ionization coefficients were performed on ten different diodes across the wafer. The mean value for $\alpha_n$ and $\alpha_p$ is provided in Figure 6.5 with the standard deviation due to variations from diode to diode. The small standard deviation indicates that the values are representative of the properties of bulk GaN.

The impact ionization coefficients for electrons and holes in GaN obtained as a function of

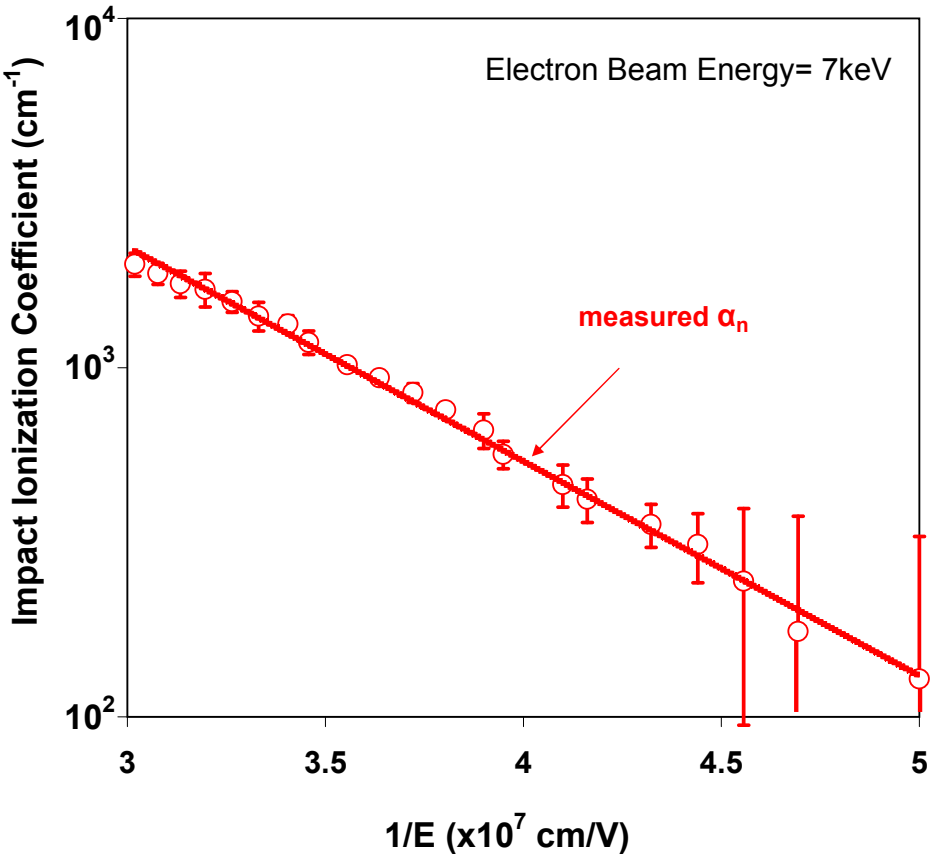


Figure 6.3: Measurement of repeatability in extraction of impact ionization coefficients.

the electric field (E) by the pulsed electron beam measurement can be fitted to Chynoweth's equation [57]:

$$\alpha = ae^{(-b/E)} \tag{6.1}$$

as shown in Figure 6.5 by the solid lines. Based upon the measurements: $a_N$ has a value of 1.5x$10^5$±(0.2x$10^5$) $cm^{-1}$ and $b_N$ has a value of 1.413x$10^7$±(0.03x$10^7$) V/cm for GaN at room temperature; $a_P$ has a value of 6.4x$10^5$±(0.1x$10^5$) $cm^{-1}$ and $b_P$ has a value of 1.454x$10^7$±(0.01x$10^7$) V/cm at room temperature.

### 6.2.3 Discussion of experimental results

Measured impact ionization data for GaN can be compared to the values reported in the literature [12][16][17] in Figure 6.6. Measured values for $\alpha_p$ are observed to be similar to those

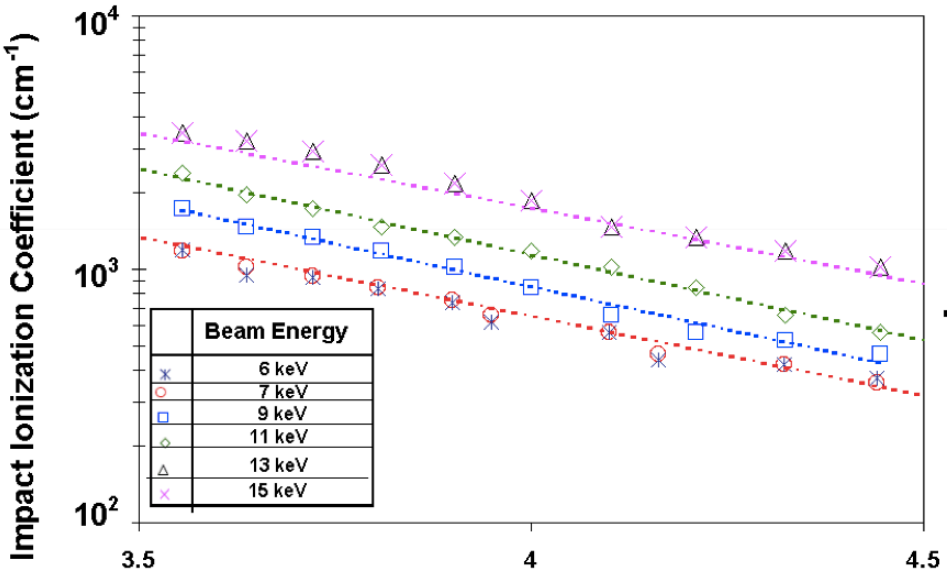


Figure 6.4: Effect of electron beam energy on the measured impact ionization coefficients in GaN.

values theoretically predicted by Oguzman [12] and significantly smaller than the measured values by McClintock [17]. Measured values for $\alpha_n$ are observed to be similar to those measured by McClintock [17] at high electric fields and considerably different from those extracted by Kunihiro [16]. The possible reasons for these differences were mentioned in the introduction.

### 6.2.4 Application of extracted impact ionization data

Instead of using Chynoweth's equation, the Fulop's power law [58]:

$$\alpha = 1.8 \times 10^{-35} E^7 \tag{6.2}$$

for the impact ionization coefficient for silicon has been found to be convenient for obtaining analytical solutions for the critical electric field and breakdown voltage for silicon devices [2]. The impact ionization coefficients for electrons have been found to be greater than the those for holes for Silicon [59]. Fulop's power law falls below that for electrons and above that for holes in silicon. It has been found to predict larger breakdown voltages than observed in numerical simulations and actual devices [60]. To resolve this problem, a Baliga's power law for silicon has been recently proposed and validated [60]:

$$\alpha = 3.507 \times 10^{-35} E^7 \tag{6.3}$$

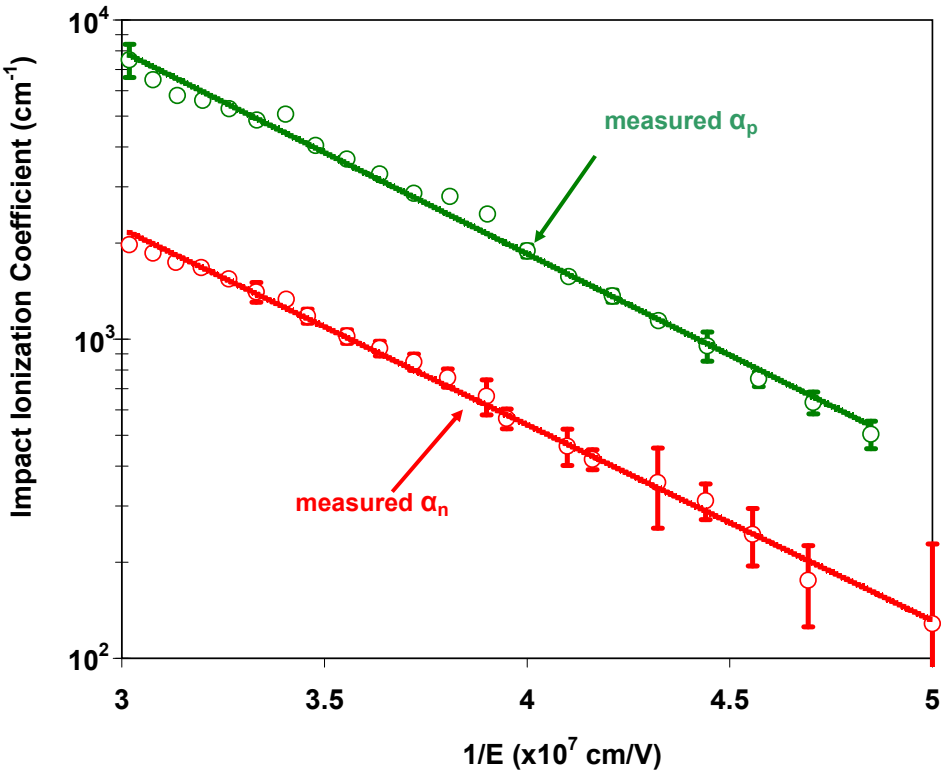


Figure 6.5: Measured impact ionization coefficients for electrons and holes in GaN using data taken at 10 diodes.

to provide a better analytical prediction of breakdown voltages in silicon devices. The Baliga power law for the impact ionization coefficient for Silicon is also less than that for electrons and greater than that for holes. A similar power law for impact ionization coefficients in GaN would be useful for analytical calculation of breakdown voltages in GaN. An Ozbek-Baliga power law for the impact ionization coefficient for GaN is proposed here:

$$\alpha = 1.5 \times 10^{-42} E^7 \tag{6.4}$$

The values for $\alpha$ for GaN obtained by using this power law equation are compared to the measured values for $\alpha_n$ and $\alpha_p$ in Figure 6.7. The impact ionization coefficients obtained using the proposed power law fall below the measured values for $\alpha_p$ and above the measured values for $\alpha_n$. Using this analytical equation for $\alpha$ in GaN, the following relationships can be derived:

Parallel-plane maximum depletion width at breakdown for GaN:

$$W_{pp} = 1.57 \times 10^{11} N_D{}^{(-7/8)} \tag{6.5}$$

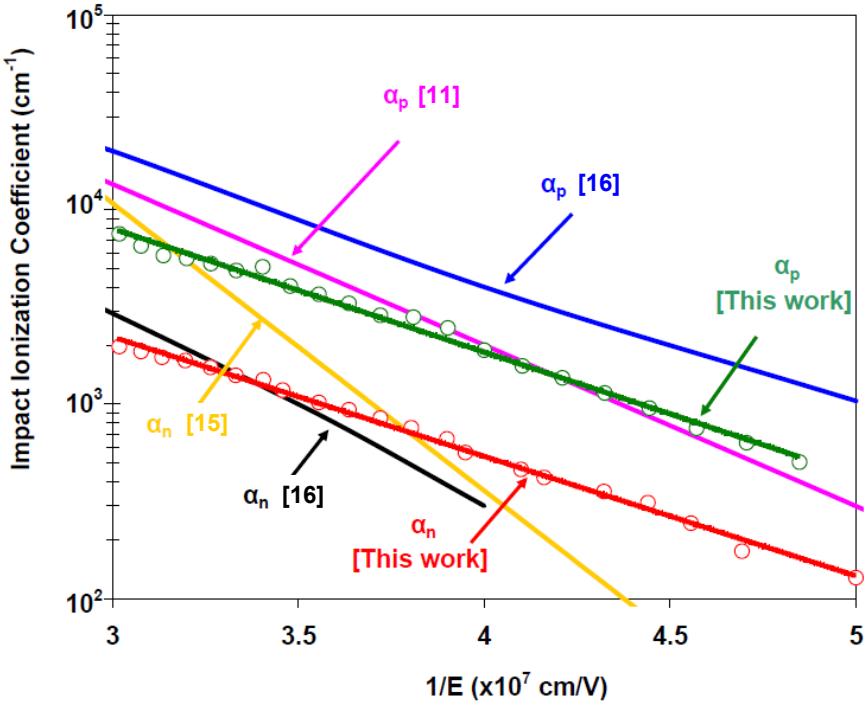


Figure 6.6: Comparison of measured impact ionization coefficients for electrons and holes in GaN at room temperature with the previous values reported in literature.

Critical electric field at breakdown for GaN:

$$E_c = 3.19 \times 10^4 {N_D}^{(1/8)} \tag{6.6}$$

Parallel-plane ideal avalanche breakdown voltage for GaN:

$$BV_{pp} = 2.51 \times 10^{15} {N_D}^{(-3/4)} \tag{6.7}$$

In order to validate the above analytically derived equations for GaN, numerical simulations of parallel-plane Schottky diode structures were performed using the extracted impact ionization coefficients [$a_n$, $b_n$, $a_p$, $b_p$] for Chynoweth's equation in the simulator. The drift region doping concentration was varied from $10^{14}$ to $10^{17}$ $cm^{-3}$. The critical electric field for breakdown in GaN obtained from the simulations is compared with the values obtained using the analytical solution [equation (6.6)] in Figure 6.8. It can be observed that there is a good match between the analytically computed values obtained using the proposed Ozbek-Baliga power law for the impact ionization coefficient in GaN and the values obtained from numerical simulations. Similarly, there is a good match between the values for the breakdown voltage and the maximum

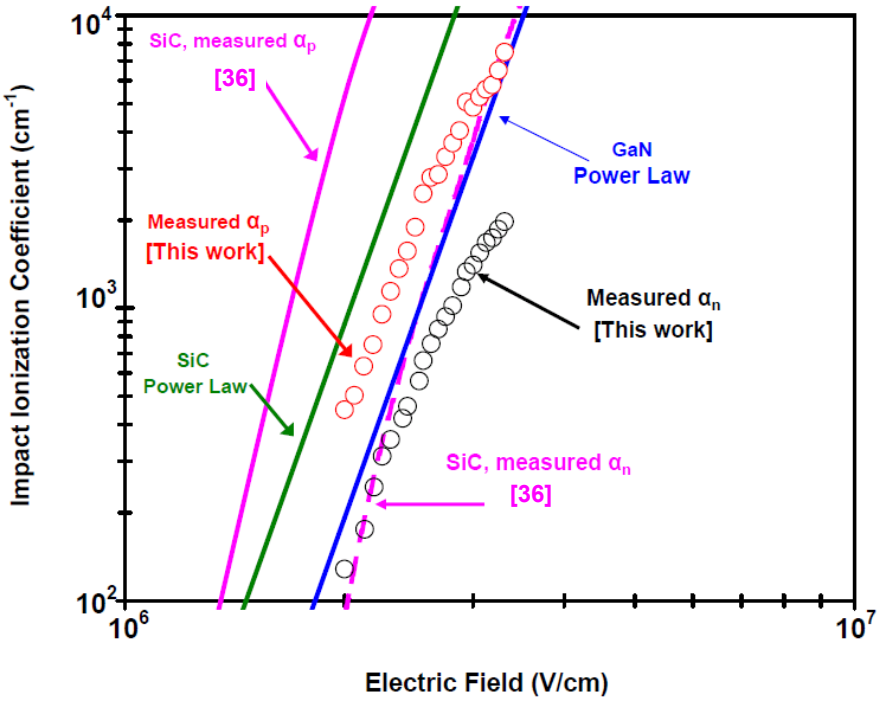


Figure 6.7: Power law approximations for the impact ionization coefficients in GaN and SiC.

depletion width obtained from the numerical simulations and the analytical solutions as shown in Figure 6.9 and Figure 6.10, respectively.

To compare the analytical solutions for GaN obtained in this work with that for SiC, analytical equations were derived for SiC by using the impact ionization coefficients measured by Konstantinov [38].The proposed power law fit for the impact ionization coefficient for SiC is:

$$\alpha = 6.9 \times 10^{-42} E^7 \tag{6.8}$$

The proposed power law fit for $\alpha$ for SiC can be compared to measured values for $\alpha_n$ and $\alpha_p$ [38] in Figure 6.7. Using this analytical equation for $\alpha$ in SiC, the following relationships can be derived:

Parallel-plane maximum depletion width at breakdown for SiC:

$$W_{pp} = 1.4 \times 10^{11} N_D{}^{(-7/8)} \tag{6.9}$$

Critical electric field at breakdown for SiC:

$$E_c = 2.61 \times 10^4 N_D{}^{(1/8)} \tag{6.10}$$

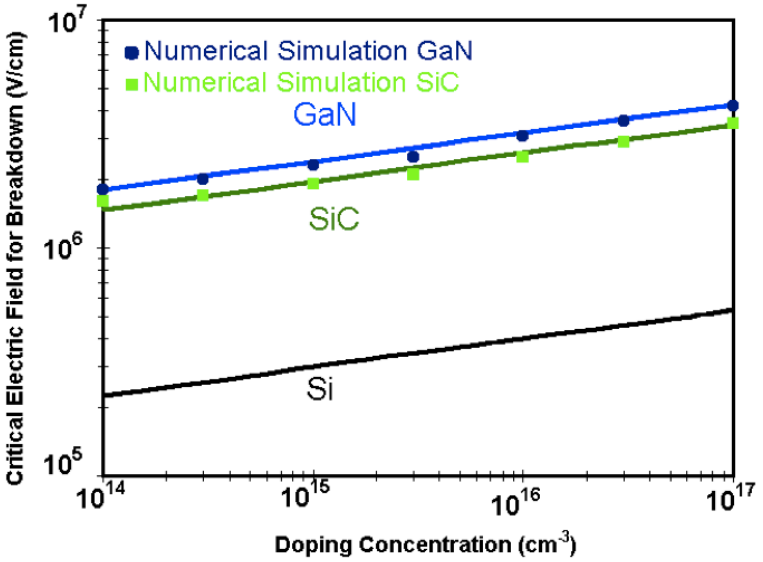


Figure 6.8: Comparison of critical electric fields for breakdown in GaN, SiC and Si.

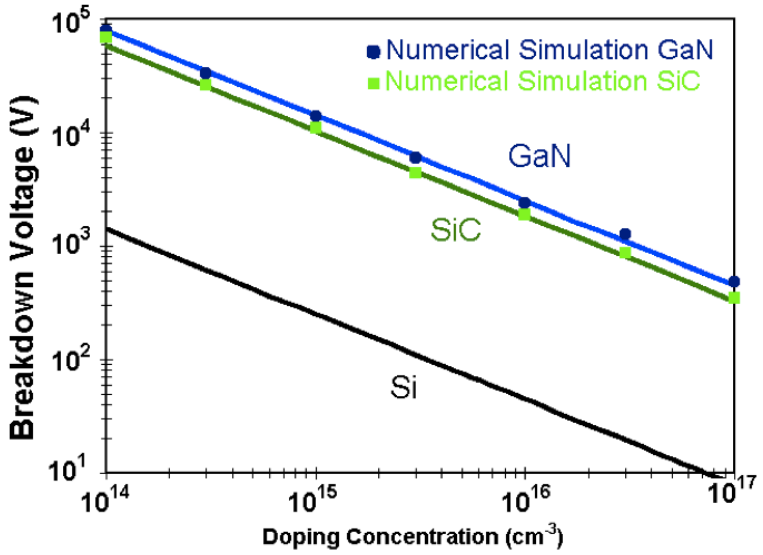


Figure 6.9: Comparison of breakdown voltages for GaN, SiC and Si.

Parallel-plane ideal avalanche breakdown voltage for SiC:

$$BV_{pp} = 1.83 \times 10^{15} N_D{}^{(-3/4)} \tag{6.11}$$

In order to validate the above analytically derived equations for SiC, numerical simulations of parallel-plane Schottky diode structures were performed using the extracted impact ionization

coefficients [$a_n$, $b_n$, $a_p$, $b_p$] for Chynoweth's equation in the simulator. The drift region doping concentration was varied from $10^{14}$ to $10^{17}$ $cm^{-3}$. The values obtained using the numerical simulations match those obtained using the above equations as shown in Figure 6.8, 6.9 and 6.10.

The critical electric field for GaN obtained in this work is compared with that for SiC and Si in Figure 6.8. It can be concluded that GaN has a critical electric field of 1.23× larger than that for SiC and 7.97× larger than that for Silicon for the same doping concentration. The breakdown voltage for GaN is compared with SiC and Si in Figure 6.9. It can be concluded that GaN has a breakdown voltage of 1.37× larger than that for SiC and 56.43× larger than that for Silicon for the same doping concentration. The maximum depletion width for GaN is compared with that for SiC and Si in Figure 6.10. It can be concluded that the depletion width for GaN is 1.12× larger than that for SiC and 6.54× larger than that for Silicon for the same doping concentration.

The specific on-resistance of the drift region for unipolar power devices is an important parameter that determines their on-state voltage drop and power loss. The specific-on resistance of the drift region is given by [60]:

$$R_{on,sp} = \frac{4BV^2}{\epsilon_s \mu_n {E_c}^3} \tag{6.12}$$

Using the above equations for the critical electric fields for GaN and SiC, the specific on-resistance for GaN can be obtained using:

$$R_{on,sp} = 3.12 \times 10^{-12} BV^{2.5} \tag{6.13}$$

and the specific on-resistance for SiC can be obtained using:

$$R_{on,sp} = 5.54 \times 10^{-12} BV^{2.5} \tag{6.14}$$

The specific on-resistance for GaN and SiC calculated by using these equations is compared to that for Si unipolar devices in Figure 6.11. The specific on-resistance for GaN unipolar devices is found to be 1.78× smaller than that for SiC devices and 2130× smaller than that for Si devices.

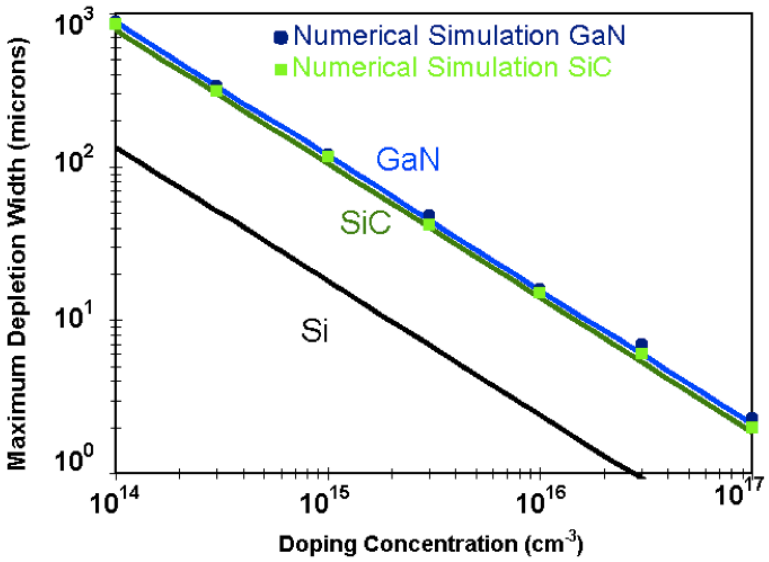


Figure 6.10: Comparison of depletion layer width at breakdown in GaN, SiC and Si.

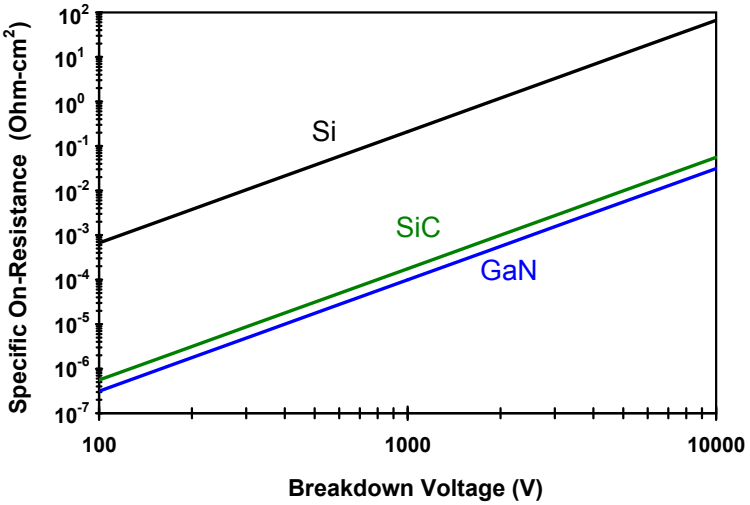


Figure 6.11: Ideal Specific On-resistance for the drift region for unipolar devices in GaN, SiC and Si.

## 6.3 Measurement of Impact Ionization Coefficients for GaN Epilayer Grown on Sapphire Substrate

### 6.3.1 Device Fabrication and Characterization

Nickel Schottky barrier diodes were fabricated on 4-$\mu$m thick n-type GaN epitaxial layers with a doping of 41014 $cm^{-3}$ grown on sapphire substrates with a 2-$\mu$m thick N+ GaN

buffer layer. Prior to the fabrication of the Schottky barrier diodes, the wafer was cleaned by trichloroethylene (5 min), acetone (5 min), methanol (5 min), and HCl:H2O (1:1) (5 min), followed by DI water flushing/N2 blow drying. The circular (150$\mu$m diameter) Schottky barrier diodes were fabricated by evaporation of 1000  of Nickel on top of the GaN epitaxial layer though a shadow mask.

As discussed in Chapter 4, argon ion implantation was performed around the edges of the GaN Schottky diodes to suppress enhancement of the electric field and to obtain nearly ideal breakdown voltage [43]. The reverse characteristics of the diode were studied using I-V measurement. The breakdown voltages were measured for a large number of diodes. Breakdown voltages as high as 1700 V were found for the terminated diodes. Macroscopic defects are known to severely affect the breakdown characteristics of devices. In the measurements, the electron beam induced current (EBIC) technique was used to first identify the location of electrically active macroscopic defects. Measurements were performed away from the macroscopic defects to extract the properties representative of GaN layers grown on sapphire substrates.

### 6.3.2 Impact Ionization Data

Extensive measurements of impact ionization coefficients were performed on ten different diodes across the wafer. The mean values for $\alpha_n$ and $\alpha_p$ are provided in Figure 6.12 together with the standard deviation observed due to variations from diode to diode. The impact ionization coefficients for electrons were extracted by using an electron-beam energy of 7keV while that for holes were extracted by using an electron-beam energy of 13keV.

The impact ionization coefficients for electrons and holes for GaN epitaxial layers grown on sapphire substrates obtained as a function of the electric field (E) by the pulsed electron beam measurement that can be fitted to Chynoweth's equation [57]: $\alpha = ae^{(-b/E)}$ as shown in Figure 6.12 by the solid lines. Based upon the measurements: $a_n$ has a value of 9.2x10$^5$(0.1x10$^5$) $cm^{-1}$ and $b_n$ has a value of 1.722x10$^7$(0.04x10$^7$) V/cm for GaN grown on sapphire substrates; $a_p$ has a value of 8.70x10$^5$(0.2x10$^5$) $cm^{-1}$ and $b_p$ has a value of 1.464x10$^7$(0.02x10$^7$) V/cm for GaN grown on sapphire substrates.

## 6.4 Comparison of Impact Ionization Data for GaN

Measured impact ionization data for GaN grown on sapphire substrates can be compared to the values reported in the literature [17] and to the values measured for GaN epitaxial layer grown on bulk GaN substrate in Figure 6.13. Measured values for $\alpha_p$ are observed to be smaller than the values measured by McClintock [17], while measured values for $\alpha_n$ are observed to be larger than those measured by McClintock [17]. Measured $\alpha_n$ and $\alpha_p$ values for GaN grown on sapphire substrates are both larger than those reported by us for GaN grown on bulk GaN

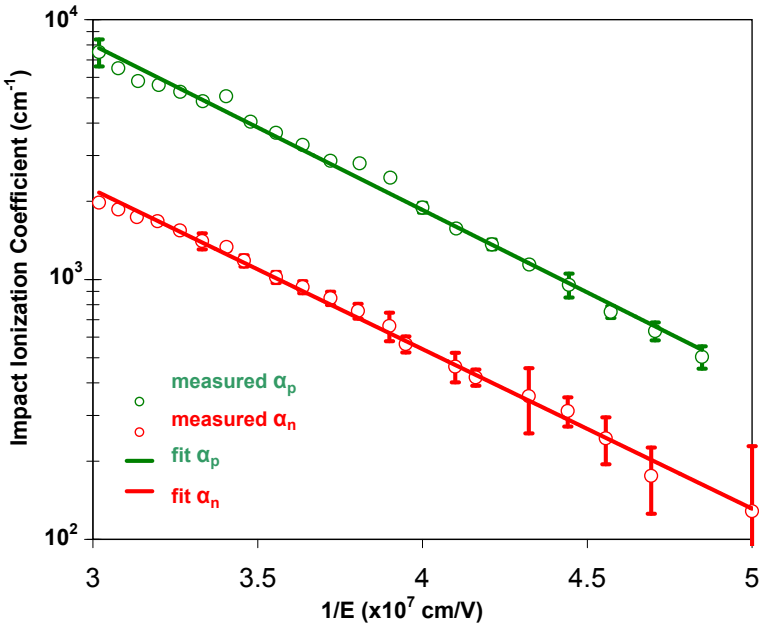


Figure 6.12: Measured impact ionization coefficients for electrons and holes in GaN using data taken at 10 diodes at room temperature.

substrates. Khan et. al. [61] have postulated that inhomogeneous disorder is responsible for the broadening of recombination lines observed in GaN grown on sapphire substrates but is absent for GaN layers grown on the GaN bulk substrates. This effect, the presence of stress, and a high dislocation density in the GaN layers grown on sapphire substrates are probable reasons for the higher values of $\alpha_n$ and $\alpha_p$ values found in this work.

## 6.5 Role of Defects on Impact Ionization in GaN

In measurements, the electron beam induced current (EBIC) measurement technique is used to identify the location of electrically active defects in GaN Schottky diodes. Unlike the conventional EBIC setup, the experimental EBIC setup was designed to allow application of high (500V) reverse biases to the GaN Schottky diodes to image defect sites with enhanced multiplication. As the electron beam rasters the surface of the device, the current induced in the semiconductor is collected by the EBIC amplifier. The data obtained from the EBIC amplifier is interfaced with a computer to digitize the data which is synchronized with the electron beam scanning circuitry. The line scan profile across the diode obtained for increasing reverse biases gives insight into the location of enhanced multiplication due to impact ionization.

A typical EBIC image of a terminated typical GaN Schottky diode at a reverse bias of 75V

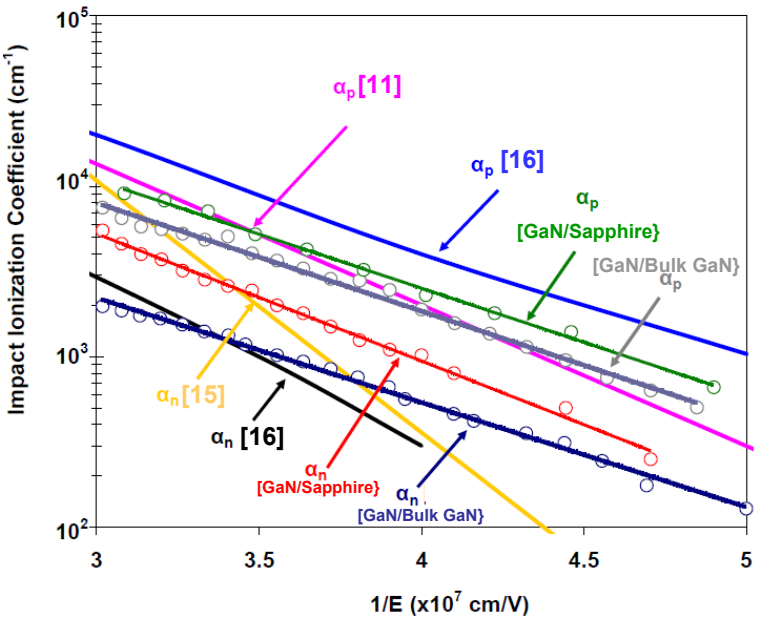


Figure 6.13: Comparison of the measured impact ionization coefficients for electrons and holes in GaN at room temperature with the previous values reported in literature.

at room temperature is shown in Figure 5.4 in chapter 5. The two bright spots in the EBIC image indicate enhanced multiplication at a defective site in the diode. Various reasons have been proposed for the high multiplication at the defect site: (a) if a defect is present in the depletion region, it could leads to enhanced multiplication by locally enhancing the electric field in it's vicinity; (b) lattice strain at the defective site could enhance multiplication due to the distortions in the band structure; (c) the defect could produce states inside the band gap that helps the transportation of carriers from the valence band to conduction band during impact ionization.

In this section, the impact ionization measurements were performed by focusing the electron beam at a defect site identified using the EBIC measurements. As explained in Chapter 3, the impact ionization coefficient for electrons can be extracted by using low electron beam energy while that for holes can be extracted by using high electron beam energy. The impact ionization coefficient for electrons obtained by using an electron beam energy of 7keV is shown in Figure 6.14 while that for holes obtained by using an electron beam energy of 13keV is shown in Figure 6.15. In both figures, the impact ionization coefficient at a defect-free site is included for comparison. It can be observed that the measured impact ionization coefficients are much larger ($\approx$5 times) at the defect site when compared to the defect free location at any electric field in the depletion region.

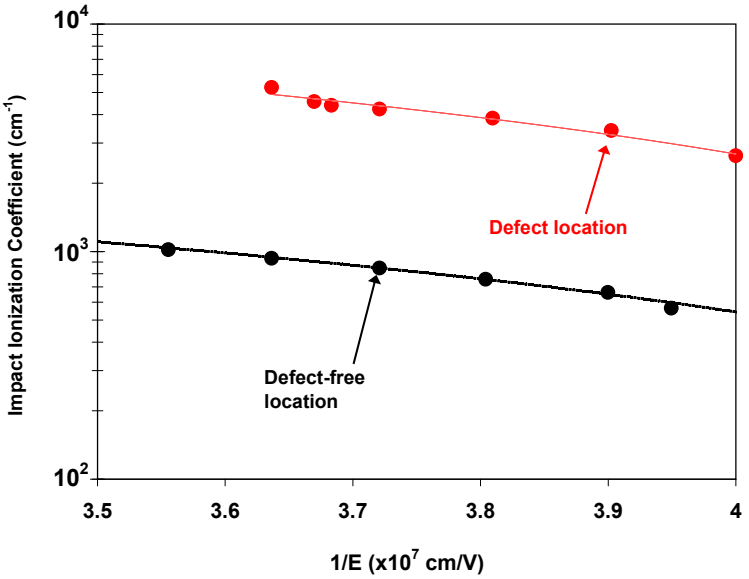


Figure 6.14: Impact Ionization coefficients for electrons in GaN measured at a defect site compared to those measured at defect-free location.

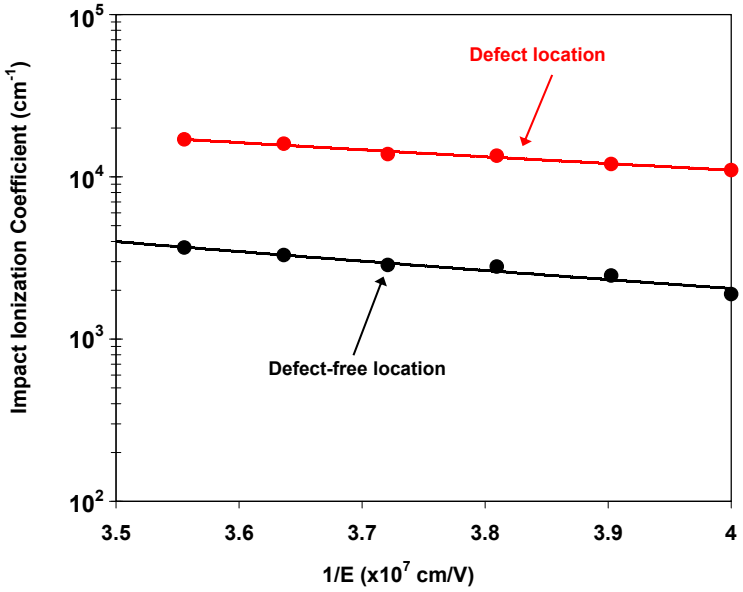


Figure 6.15: Impact Ionization coefficients for holes in GaN measured at a defect site compared to those measured at defect-free location.

In measurements, it is demonstrated that the impact ionization coefficients measured at defective site in GaN are much larger than at defect-free sites. This indicates that the presence

of defects in GaN material will degrade the breakdown voltage of devices. Cao et. al. [62] have reported that GaN PiN rectifiers on a free-standing GaN show high reverse leakage and premature breakdown due to the presence of point and microdefects in the voltage-blocking layer. Cao et. al. concluded that the microdefects are believed to originate from the substrate surface and point defects in GaN, including common impurities (C, H, and O), N and Ga vacancies and antisites may act as dopants or compensation centers.

## 6.6 Temperature dependence of impact ionization coefficients in GaN

Conflicting temperature dependencies of breakdown voltages for GaN power devices have been reported [18][19][20][21][22]. Earlier reports by Tan et. al. [18], Johnson et al. [20] and Zhong et al. [21] indicated negative temperature coefficient for breakdown in GaN. However, Dykonova et al. [19] and Dmitriev et al. [22] indicate positive temperature coefficients for breakdown in GaN. In this section, the temperature dependence of the impact ionization coefficients for electrons and holes for GaN as a function of electric field are reported for the first time by using measurements performed with the pulsed electron beam technique. The measurements have been conducted for GaN layers grown on GaN substrates and for GaN layers grown on sapphire substrates.

The use of a sample heater within the SEM made it feasible to perform measurements up to temperatures as high as 400 K allowing us to obtain impact ionization coefficients as a function of temperature. The measured impact ionization coefficients obtained in GaN epitaxial layers grown on bulk GaN substrates as a function of electric field at various temperatures are shown in Figure 6.16 for electrons and in Figure 6.17 for holes. It can be observed that the impact ionization coefficient for both electrons and holes reduces when the temperature is increased from 300 K to 375 K. The Chynoweth's coefficients (a, b) calculated at each temperature for GaN epitaxial layers grown on bulk GaN substrates is plotted in Figure 6.18 and Figure 6.19. The extracted values for the coefficients an and ap are :

$$a_n = 4.42x10^5 - 9.73x10^2T \tag{6.15}$$

$$a_p = 1.68x10^6 - 3.44x10^3T \tag{6.16}$$

based upon the solid lines in Figure 6.18 where T is the temperature in degrees Kelvin. In Figure 6.19, the coefficients $b_n$ and $b_p$ are observed to be independent of temperature within experimental tolerances. The extracted values for the coefficients $b_n$ and $b_p$ are 1.413x$10^7$ V/cm and 1.454x$10^7$ V/cm.

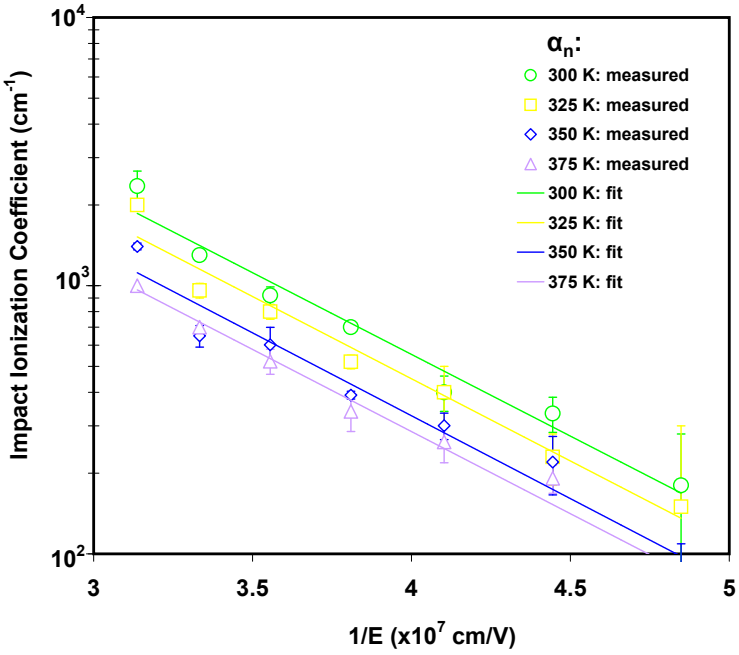


Figure 6.16: Measured electron impact ionization coefficients for GaN epitaxial layer grown on bulk GaN substrate at temperatures ranging from 300 K to 375 K.

The measured impact ionization coefficients obtained in GaN epitaxial layers grown on sapphire substrates as a function of electric field at various temperatures are shown in Figure 6.20 for electrons and in Figure 6.21 for holes. It can be observed that the impact ionization for both electrons and holes reduces when the temperature is increased from 300 K to 375 K. The Chynoweth's coefficients (a, b) calculated at each temperature for GaN epitaxial layers grown on sapphire substrates is plotted in Figure 6.22 and Figure 6.23. The extracted values for the coefficients an and ap are:

$$a_n = 2.82x10^6 - 6.34x10^3T \tag{6.17}$$

$$a_p = 2.98x10^6 - 7.02x10^3T \tag{6.18}$$

based upon the solid lines in Figure 6.22 where T is the temperature in degrees Kelvin. In Figure 6.23, the coefficients $b_n$ and $b_p$ are observed to be independent of temperature within experimental tolerances. The extracted values for the coefficients $b_n$ and $b_p$ are 1.722x$10^7$ V/cm and 1.464x$10^7$ V/cm.

The observed negative temperature coefficient for impact ionizations for GaN epitaxial layers grown on both bulk GaN and sapphire substrates implies an increase in breakdown voltage with temperature. To verify this, the breakdown voltage of the argon implant terminated Schottky

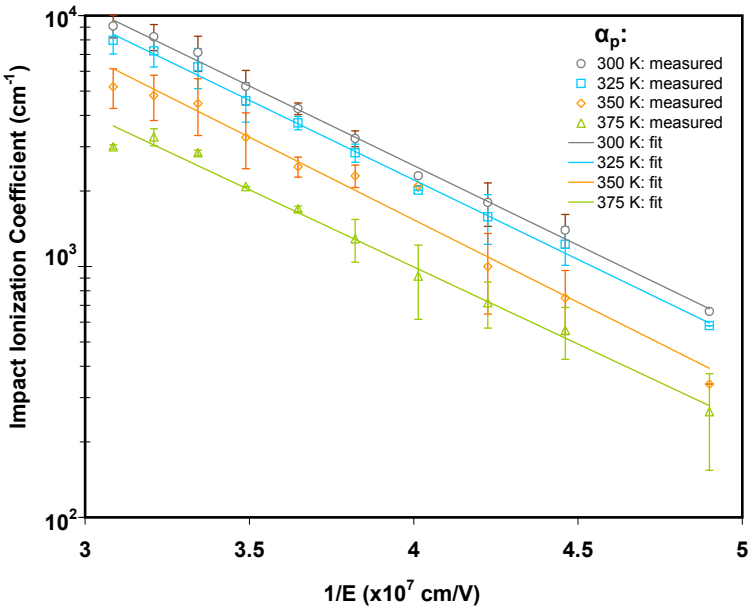


Figure 6.17: Measured hole impact ionization coefficients for GaN epitaxial layer grown on bulk GaN substrate at temperatures ranging from 300 K to 375 K.

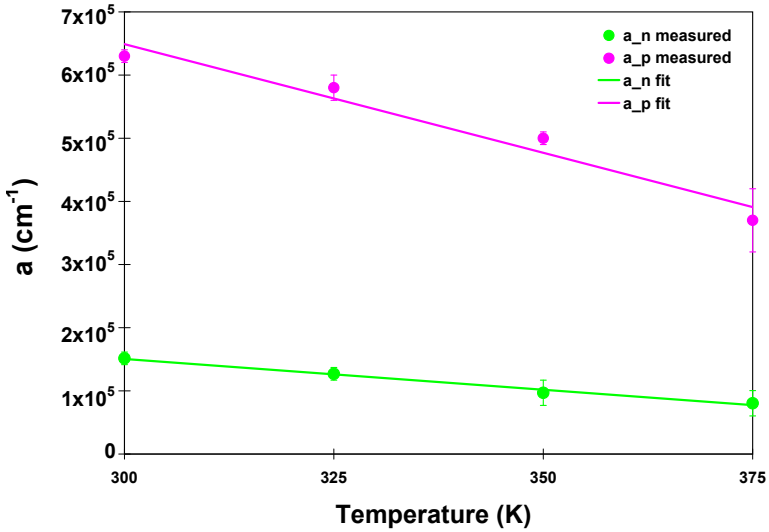


Figure 6.18: Temperature dependence of the coefficients $a_n$ and $a_p$ for GaN epitaxial layer grown on bulk GaN substrate.

diodes was measured as a function of temperature. The breakdown voltage data in Figure 6.24 for GaN epitaxial layers grown on both bulk GaN and sapphire substrates shows an increase in breakdown voltage with temperature consistent with the measured decrease in the impact

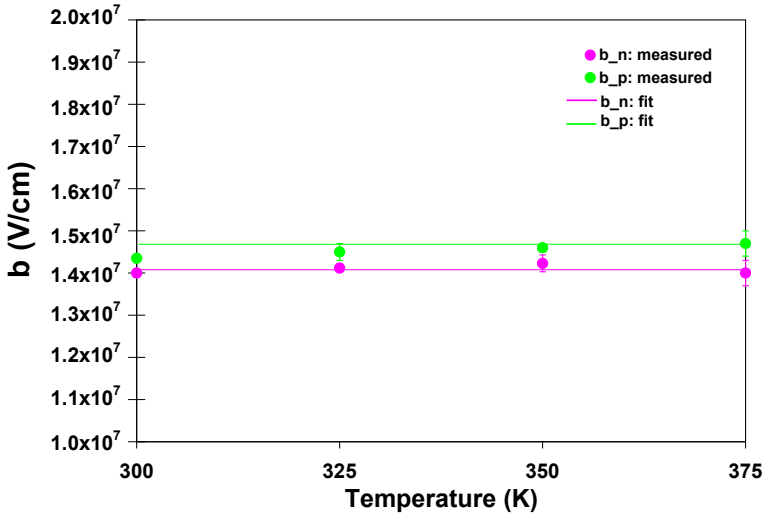


Figure 6.19: Temperature dependence of the coefficients $b_n$ and $b_p$ for GaN epitaxial layer grown on bulk GaN substrate.

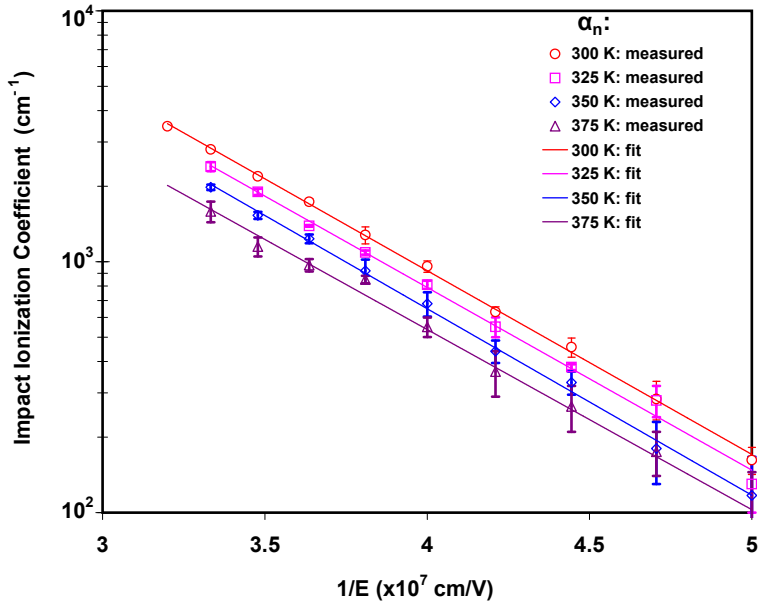


Figure 6.20: Measured electron impact ionization coefficients for GaN epitaxial layer grown on Sapphire substrate at temperatures ranging from 300 K to 375 K.

ionization coefficients with temperature. The increase in breakdown voltage of GaN devices with increasing temperature is an important desirable characteristic as this ensures stable and reliable behavior for GaN power devices.

The negative temperature coefficient dependence is because of the increased lattice scat-

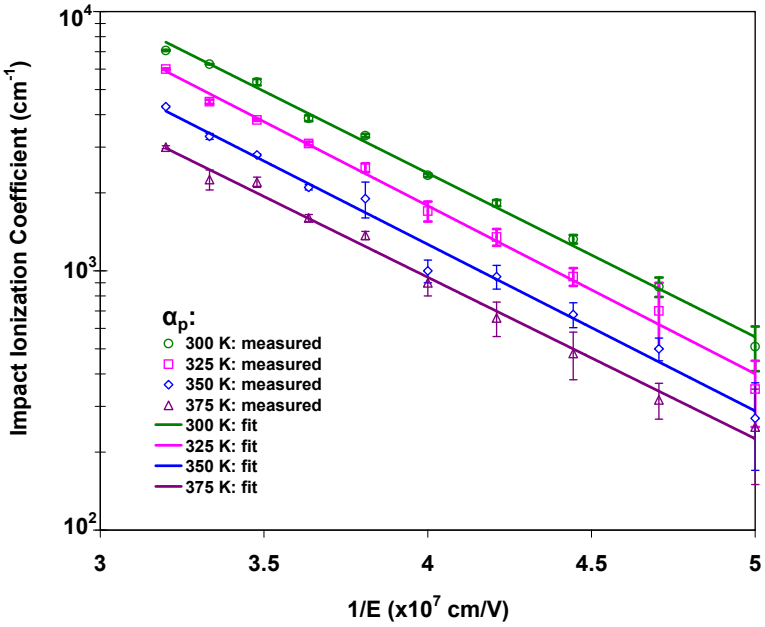


Figure 6.21: Measured hole impact ionization coefficients for GaN epitaxial layer grown on Sapphire substrate at temperatures ranging from 300 K to 375 K.

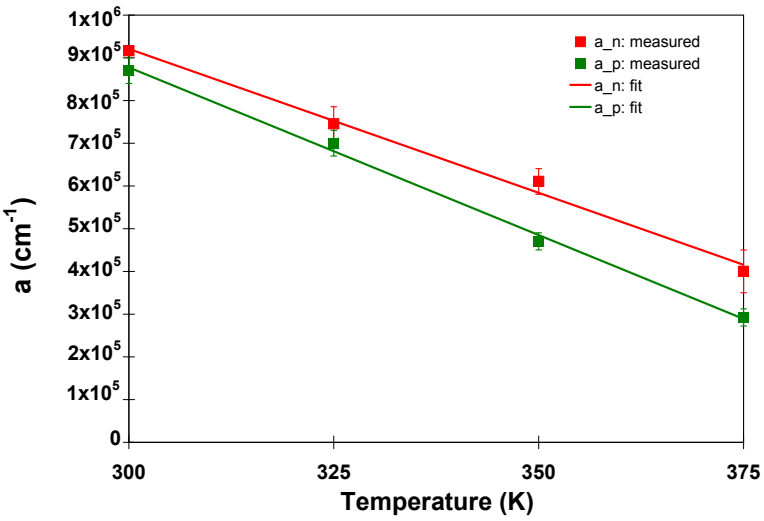


Figure 6.22: Temperature dependence of the coefficients $a_n$ and $a_p$ for GaN epitaxial layer grown on sapphire substrate.

tering at elevated temperatures. Impact ionization is suppressed by increasing temperature due to the increase in lattice scattering which originates from thermal vibrations of the lattice atom at high temperatures. These vibrations disturb the lattice periodic potential and allow

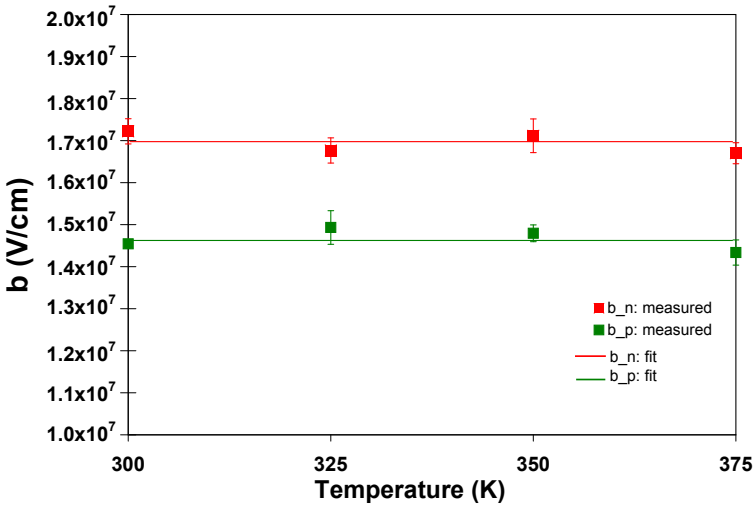


Figure 6.23: Temperature dependence of the coefficients $b_n$ and $b_p$ for GaN epitaxial layer grown on sapphire substrate.

energy transfer between the carriers and the lattice. Lattice vibration amplitude increases with rising temperature. This causes increased probability of scattering of carriers from lattice and reduces the mean free path between scattering events which reduces the total energy gained by the carriers between scattering events at any fixed electric field making the impact ionization coefficients smaller.

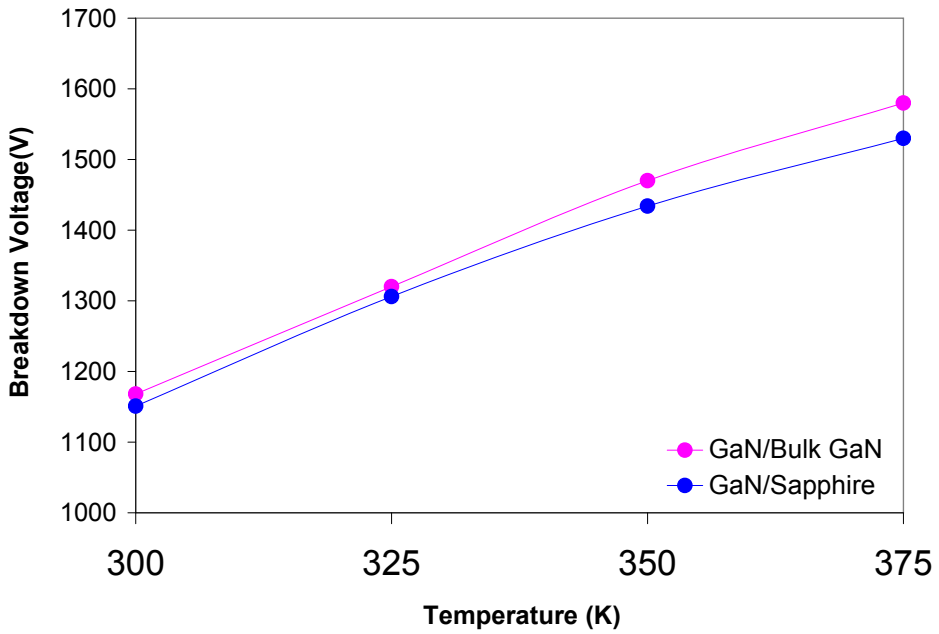


Figure 6.24: Measured increase of breakdown voltage with increasing temperature for both GaN epitaxial layer grown on bulk GaN substrate and GaN epitaxial layer grown on Sapphire substrate.

# Chapter 7

# Conclusion and Future Work

Electron and hole impact ionization coefficients have been measured for the first time in GaN epitaxial layers grown on bulk GaN substrates by using a pulsed electron beam technique. For Chynoweth's equation, measurements gave an $a_N$ value of 1.5x10$^5$ $cm^{-1}$ and a value of $b_N$ of 1.41x10$^7$ V/cm for the impact ionization coefficient for electrons in GaN at room temperature. For the impact ionization coefficients for holes in GaN at room temperature, the values of $a_P$ and $b_P$ were found to be 6.4x10$^5$ $cm^{-1}$ and 1.46x10$^7$ V/cm, respectively. Using these coefficients, analytical models for the critical electric field for breakdown, the breakdown voltage, and the specific on-resistance for GaN have been developed.

Electron and hole impact ionization coefficients have been also measured for GaN epitaxial layers grown on sapphire substrates by using a pulsed electron beam technique. For Chynoweth's equation, measurements gave an $a_N$ value of 9.17x10$^5$ $cm^{-1}$ and a value of $b_N$ of 1.72x10$^7$ V/cm for the impact ionization coefficient for electrons at room temperature. For the impact ionization coefficients for holes at room temperature, the values of $a_P$ and $b_P$ were found to be 8.7x10$^5$ $cm^{-1}$ and 1.46x10$^7$ V/cm, respectively. The values for both coefficients are larger than those measured for GaN grown on GaN substrates.

The role of defects on impact ionization in Gallium Nitride has been investigated. EBIC images of GaN Schottky Rectifiers with high reverse bias voltages showed that defects cause enhanced multiplication at local sites. A pulsed electron beam technique was used to extract the impact ionization coefficients for holes and electrons at sites identified to contain defects by the EBIC measurements. The impact ionization coefficients for holes and electrons measured at the defect site were found to be significantly larger (≈5x) than those measured at defect-free sites. These results indicate that the breakdown voltage of GaN devices can be reduced due to the presence of defects.

The role of temperature variation on electron and hole impact ionization coefficients have been accurately measured as in both GaN epitaxial layer grown on bulk GaN substrate and

GaN epitaxial layer grown on Sapphire substrate by using a pulsed electron beam technique. The results show that the breakdown voltage of GaN devices is predicted to increase with temperature coefficient due to a decrease of the coefficient a in the Chynoweth's equation.

Recently, AlGaN/GaN heterojunction field effect transistors (HFETs) have been under extensive investigation because of their projected superb performances as high-power RF devices. The inherently high breakdown field arising from the wide bandgap guarantees not only the high power input/output characteristics [63][64][65] but also extreme device shrinkage which is a huge advantage for increasing the highest operation frequency [66]. Two-dimensional electron gas (2-DEG) with the charge density ten times higher than that of GaAs-based HFETs and the mobility well exceeding Si enables a very low on-state resistance indispensable to RF devices [67]. Consequently, the application field has been extended from high-power amplifiers for base-stations [68] to high-power [69] and low-noise amplifiers in millimeter-wave regimes. In addition, such material advantages for low and high breakdown voltages have driven another motivation to apply AlGaN/GaN HFETs to high-power switching devices [70][71][72][73].

Although the superiority of the device characteristics to those of SiC and Si MOSbased devices has been demonstrated, limited availability of high-quality epitaxial layers applicable to electron devices realized only on SiC or sapphire substrates has hindered low cost production of high power and high speed GaN-based switching devices. In this respect, Si is gaining more interest as an alternative substrate because of its low-cost, large wafer size, and high crystal quality. To date, several groups have succeeded in fabricating GaN-based photonic and electronic devices such as LEDs, UV detectors and high electron mobility heterostructures on Si substrates [74]. Therefore, the future work can focus on the measurement of impact ionization coefficients for GaN grown epitaxial layers on Silicon substrates.

## REFERENCES


[1] Baliga, B. J. *Silicon carbide power devices* World Scientific, 2005.

[2] Baliga, B. J. *Fundamentals of Power Semiconductor Devices* New York, USA: Springer, 2008.

[3] Baliga, B. J. *Power semiconductor device figure of merit for high-frequency applications*, IEEE Electron Device Letters, 10(10):455-457, 1989.

[4] Mishra, U. K., Shen, L., Kazior, T. E. and Y. W. *GaN-Based RF Power Devices and Amplifiers* Proceedings of the IEEE, 96(2):287-305, 2008.

[5] Rumyantsev, M., Bougrov, V., Levinshtein, V. and Zubrilov, A. *Properties of Advanced Semiconductor Materials GaN, AlN, InN, BN, SiC, SiGe* John Wiley and Sons Inc, 2001.

[6] Jin, Y. *Simulation methodology to compare emerging technologies for alternatives to silicon gigascale logic device* Ph. D. Dissertation, NC State University, 2006.

[7] Paskove, T. *Progress, Status and Prospects* IEEE Journal of Selected Topics in Quantum Electronics, 15(4):10411052, 2009.

[8] Xu, X. *Growth and characterization of low defect GaN by hydride vapor phase epitaxy* Journal of Crystal Growth, 246:223229, 2002.

[9] Mion, C. *Accurate dependence of gallium nitride thermal conductivity on dislocation density* Applied Physics Letters, 89, 2006.

[10] Pearton, S. J. *Fabrication and performance of GaN electronic devices* Materials Science and Engineering, 30:55212, 2000.

[11] Kolnik, J., Oguzman, I. H., Brennan, K., Wang, R. and Ruden, P. *Monte Carlo calculation of electron initiated impact ionization in bulk zinc-blende and wurtzite GaN* Journal of Applied Physics, 81:726733, 1997.

[12] Oguzman, I. H., Bellotti, E., Brennan, K.F., Kolnik, J. and Ruden, P. P. *Theory of hole initiated impact ionization in bulk zincblende and wurtzite GaN*, Journal of Applied Physics, 81:78277834, 1997.

[13] Cao, J. C. and Lei, X. L. *Nonparabolic multivalley balance-equation approach to impact ionization : Appication to wurtzite GaN* European Physics Journal, 7:7983, 1999.

[14] Chen, S and Wang, G. *High-field properties of carrier transport in bulk wurtzite GaN: A Monte Carlo perspective* Journal of Applied Physics, 7:23703-1 - 23703-6, 2008.

[15] Bertazzi, F., Moresco, M. and Bellotti, E. *Theory of high-field carrier transport and impact ionization in wurtzite GaN. Part I: A full band Monte Carlo model* Journal of Applied Physics, 106:063718-1 - 063718-12 , 2009.

[16] Kunihiro, K., Kasahara, K., Takahashi, Y. and Ohno, Y. *Experimental Evaluation of Impact Ionization Coefficients in GaN* IEEE Electron Device Letters, 20:608-610, 1999.

[17] McClintock, R., Pau, J. L., Minder, K. Bayram, C., Kung, P. and Razeghi, M. *Hole-initiated muliplication in back-illuminated GaN avalanche photodiodes* Applied Physics Letters, 90:141112-1 - 141112-3, 2007.

[18] Tan, W. S., Houston, P. A., Parkbrook, P. J., Wood, D. A., Hill, G. and Whitehouse, C. R. *Gate leakage effects and breakdown voltage in metalorganic vapor phase epitaxy AlGaN-GaN heterostructure field-effect transistors* Applied Physics Letters, 80(17):3207-3211, 2002.

[19] Dyakonova, N., Dickens, A., Shura, M. S., Gaska, R. and Yang, J. W. *Temperature dependence of impact ionization in AlGaN-GaN heterostructure field effect transistors* Applied Physics Letters, 72(20):2562-2564, 1998.

[20] Johnson, J. W., LaRoch, J. R., Fen, F., Gilla, B. P., Overberg, M. E., Abernathy, C. R., Chyi, J. I., Cuo, C. C., Nee, T. E., Lee, C. M., Lee, K. P., Park, S. S., Park, Y. J. and Pearton, S. J. *Schottky rectifiers fabricated on free-standing GaN substrates* Solid State Electronics, 45:405-410, 2001.

[21] Zhang, A. P., Dang, G. T., Ren, F., Cho, H., Lee, K. P., Pearton, K. P., Chyi, J. I., Nee, T.-E., Lee, C.M. and Chuo, C.C. *Comparison of GaN P-I-N and Schottky Rectifier Performance* IEEE Transactions on Electron Devices, 48(3):407-412, 2001.

[22] Dmitriev, V. A., Irvine, K. G., Carter, C. H., Kuznetsov, N. I. and Kalinin ,E. V *lectric breakdown in GaN p-n junctions* Applied Physics Letters, 68(2):229-232, 1996.

[23] McKay, K.G. and McAfee, K. B. *Electron Multiplication in Silicon and Germanium*, Phys. Rev., 91:1079 1953.

[24] McKay, K. G. *Avalanche Breakdown in Silicon*, Phys. Rev., 94:877, 1954.

[25] Wolff, P. A. *Theory of Electron Multiplication in Silicon and Germanium*, Phys. Rev., 95:1415, 1954.

[26] Miller, S. L. *Ionization Rates for Holes and Electrons in Silicon*, Phys. Rev. 105:1246, 1957.

[27] Chynoweth, A. G. and McKay, K. G. *Threshold Energy for Electron-Hole Pair Production by Electrons in Silicon*, Phys. Rev., 108:29, 1957.

[28] Chynoweth, A. G., *Ionization Rates for Electrons and Holes in Silicon*, Phys. Rev., 109:1537, 1958.

[29] Chynoweth, A. G. and Pearson, G. L. *Effect of Dislocations on Breakdown in Silicon p-n Junctions*, Journal of Applied Physics, 29:1103, 1958.

[30] Chynoweth, A. G., *Uniform Silicon p-n Junctions. II. Ionization Raes for Electrons*, Journal of Applied Physics, 31:1161, 1960.

[31] Shockley, W., *Problems Related To p-n Junctions in Silicon*, Solid State Electronics, 2:35, 1961.

[32] Baraff, G. A., *Distribution Functions and Ionization Rates for Hot Electrons in Semiconductors*, Physics Review, 128:2507, 1962.

[33] Moll, J. L. and Overstraeten, R. V. *Charge Multiplication in Silicon p-n Junctions*, Solid State Electronics, 6:147, 1963.

[34] Lee, C. A., Logan, R. A., Batdorf, R.L., Kleimack, J. J. and Weigmann, W., *Ionization Rates of Holes and Electrons in Silicon*, Physics Review, 134:761, 1964.

[35] Opdorp, C. V. and Vrakking, J. *Avalanche Breakdown in Epitaxial SiC p-n Junctions*, Journal of Applied Physics, 40:2320, 1969.

[36] Glover, G. H. *Charge multiplication in Au-SiC (6H) Schottky junctions*, Journal of Applied Physics, 46:4842, 1975.

[37] Raghunathan, R. and Baliga, B. J., *Measurement of Electron and Hole Impact Ionization Coefficients for SiC*, Proc. of Intl. Symp. on Semiconductor Power Devices, 173, 1997.

[38] Konstantinov, A. O., Wahab, Q., Nordell, N. and Lindefelt, U., *Study of Avalanche Breakdown and Impact Ionization in 4H silicon Carbide*, Journal of Electronic Materials, 27:335, 1998.

[39] Raghunathan, R. and Baliga, B. J., *Role of defects in producing negative temperature dependence of breakdown voltage in SiC*, Applied Physics Letters, 72:3196, 1998.

[40] Hatakeyama, T., Watanabe, T., Shinohe, T., Kojima, K., Arai, K. and Sano, N, *Impact ionization coefficient of 4H silicon carbide*, Appl. Phys. Letters, 85:1380, 2004.

[41] Loh, W.S., Ng, B.K. , Ng, J.S., Soloviev, S., Cha, H., Sandvik, P., Johnson, C. M. and Daid, J. P. R., *Impact ionization coefficients in 4H-SiC*, IEEE Transactions on Electron Devices, 55:1984, 2008.

[42] Hui, K., Hu, C., George, P. and Ko, P. K., *Impact Ionization in GaAs MESFET's*, IEEE Electron Device Letters, 11(3):113-115, 1990.

[43] Ozbek, A. M. and Baliga, B. J., *Planar, nearly ideal edge termination technique for GaN devices*, IEEE Electron Device Letter., 32(3):300302, 2011.

[44] Sze, S. M. and Ng, K. K., *Physics of Semiconductor Devices*, John Wiley Sons Inc., Hoboken,New Jersey, 2007.

[45] Schroder, D. K., *Semiconductor material and device characterization*, John Wiley Sons Inc., Hoboken,New Jersey, 2006.

[46] Chow,T. P., Khemka, V., Fedison, V., Ramulgul, N., Matocha, K., Tang, Y. and Gutmann, R. J. *SiC and GaN bipolar devices*, Solid State Electronics, 44:277-301, 2000.

[47] Bandic, Z. Z, Bridger, P. M., Piquette, E. C., McGill, T. C., Vaudo, R. P., Phanse, V.M. and Redwing, J. M., *High voltage (450 V) GaN Schottky rectifiers*, Applied Physics Letters, 74(9):1266-1268, 1999.

[48] Zhang, A. P., Johnson, J. W., Luo, B., Ren, F., Pearton, S. J., Park, S. S., Park, Y. J. and Chyi, J. I., *Vertical and lateral GaN rectifiers on free standing GaN sunbstrates*, Applied Physics Letters, 79(10):1555-1557, 2001.

[49] Laroche, J. R., Ren, F., Baik, K. W., Pearton, S. J., Shelton, B. S. and Peres, B., *Design of Edge Termination for GaN Power Schottky Diodes*, Journal of Elect. Mat., 34(4):370-374, 2005.

[50] Baik, H. K., Irokawa, Y., Ren, F., Pearton, S. J., Park, S. S. and Park, Y. J., *Design of junction termination structures for GaN Schottky power rectifiers*, Solid State Electronics, 47:975-979, 2003.

[51] Ip, K., Baik, K. H., Luo, B., Ren, F., Pearton, S. J., Park, S. S., Park, Y. J. and Zhang, A. P., *High current bulk GaN Schottky rectifiers*, Solid State Electron., 46:2169-2172, 2002.

[52] Alok, D., Baliga, B. J. and McLarty, P. K., *A Simple Edge Termination for Silicon Carbide Devices with Nearly Ideal Breakdown Voltages*, IEEE Electron Device Letters, 15:394-395, 1994.

[53] Alok, D., Raghunathan, R. and Baliga, B. J., *Planar Edge Termination for 4H-Silicon Carbide Devices*, IEEE Transactions on Electron Devices , 43:1315-1316, 1996.

[54] Mohammed, S. N., Fan, Z., Botchkarev, A. E., Kim, W., Aktas, O., Salvador, A. and Morkoc, H., *Near-ideal platinum-GaN Schottky diodes*, IEEE Transactions on Electron Devices, 32(6):598-599, 1996.

[55] Zhou, Y., Li, M., Wang, D., Ahyi, C., Tin, C.C., Williams, J., Minseo, P., Williams, N. M. and Hanser, A., *Electrical characteristics of bulk GaN-based Schottky rectifiers with ultrafast reverse recovery*, Appl. Phys. Lett., 88:113509, 2006.

[56] Jiang, D., Zhao, D. and Yang, H. *Optical analysis of dislocation-related physical processes in GaN-based epilayers*, Phys. Stat. Sol., 244(8):28782891, 2007.

[57] Chynoweth, A. G., *Uniform Silicon p-n Junctions. II. Ionization Rates for Electrons*, Journal of Applied Physics,31(7):1161-1165, 1960.

[58] Fulop, W., *Calculation of avalanche breakdown voltages of silicon pn junctions*, *Solid State Elect.*, 10:39-43, 1967.

[59] Van Overstraeten, R. and De Man, H., *Measurement of the ionization rates in diffused silicon p-n junctions*, Solid State Elect.,13:583-608, 1970.

[60] Baliga, B. J., *Advanced Power MOSFET Concepts*, *Springer*,New York, 2010.

[61] Khan, M. A., Yang, J. W., Knap, W., Frayssinet, E., Hu, X., Simin, G., Prystawko, P., Leszczynski, M., Grzegory, I., Porowski, S., Gaska, G., Shur, M. S., Beaumont, B., Teisseire, M. and Neu, G., *GaN-AlGaN heterostructure field-effect transistors over bulk GaN substrates*, Appl. Phys. Lett., 76(25):3807-3809, 2000.

[62] Cao, X. A., Lu, H., LeBoeuf, S. F., Cowen, C., Arthur, S. D. and Wang, W., *Growth and characterization of GaN Pin rectifiers on free-standing GaN*, Appl. Phys. Lett., 87:053503-1 - 053503-3, 2005.

[63] Joshin, K., Kikkawa, T., Hayashi, H., Maniwa, T., Yokokawa, S., Yokoyama, M., Adachi, N. and Takikawa, M., *A 174 W high-efficiency GaN HEMT power amplifier for W-CDMA base station applications,*, IEDM Tech. Dig., 983985, 2003.

[64] Quay, R., Tessman, A., Kiefer, R., Weber, R., Van Raay, F., Kuri, M., Riessle, M., Massler, H., Muller, S., Schlechtweg, M. and Weimann, G., *AlGaN/GaN HEMTs on SiC: Toward power operation at V-band,*, IEDM Tech. Dig., 567570, 2003.

[65] Ishida, H., Hirose, Y., Murata, T., Kanda, A., Ikeda, Y., Matsuno, T., Inoue, K., Uemoto, Y., Tanaka, T. and Ueda, D., *A high power Tx/Rx switch IC using AlGaN/GaN HFETs,*, IEDM Tech. Dig., 583586, 2003.

[66] Ohno, Y. and Kuzuhara, M. *Application of GaN-based heterojunction FETs for advanced wireless communication,*, IEEE Trans. Electron Devices, 48(5):517523, 2001.

[67] Ambacher, O., Smart, J., Shealy, J. R., Weimann, N. G., Chu, K., Murphy, M., Schaff, W. J., Eastman, L. F., Dimitrov, R., Wittmer, L., Stutzmann, M., Rieger, W. and Hilsenbeck, J. *Two-dimensional electron gases induced by spontaneous and piezoelectric polarization charges in N- and Ga-face AlGaN/GaN heterostructures,*, J. Appl. Phys., 85:32223233, 1999.

[68] Ando, Y., Okamoto, Y., Hataya, K., Nakayama, T., Miyamoto, H., Inoue, T. and Kuzuhara, M. *12 W/mm recessed-gate AlGaN/GaN heterojunction field-plate FET,*, IEDM Tech. Dig., 563566, 2003.

[69] Boutros, K., Regan, M., Rowell, P., Gotthold, R., Birkhahn, R. and Brar, B. *High performance GaN HEMTs at 40 GHz with power density of 2.8 W/mm,*, IEDM Tech. Dig., 981983, 2003.

[70] Zhang, N. Q., Moran, B., DenBaars, S. P., Mishra, U. K., Wang, X. W. and Ma, T. P. *ffects of surface traps on breakdown voltage and switching speed of GaN power switching HEMTs,*, IEDM Tech. Dig., 589592, 2001.

[71] Yoshida, S., Ishii, H., Li, J., Wang, D. and Ichiwaka, M. *A high-power AlGaN/GaN heterojunction field-effect transistor,*, Solid State Electron., 47:589592, 2003.

[72] Saito, W., Takada, Y., Kuraguchi, M., Tsuda, K., Omura, I. and Ogura, T. *600 V AlGaN/GaN power-HEMT: Design, fabrication and demonstration on high voltage DC-DC converter,*, IEDM Tech. Dig., 587590, 2003.

[73] Iwakami, S., Yanagihara, M., Machida, O., Chino, E., Kaneko, N., Goto, H. and Ohtsuka, K. *ALGaN/GaN heterostructure field-effect transistors (HFETs) on Si substrates for large-current operation,*, Jpn. J. App. Phys., 43:831833, 2004.

[74] Hikita, M., Yanagihara, M., Nakazawa, K., Ueno, H., Hirose, Y., Ueda, T., Uemoto, Y., Tanaka, T., Ueda, D. and Egawa, T. *AlGaN/GaN Power HFET on Silicon Substrate With Source-Via Grounding (SVG) Structure,*, IEEE Trans. ON Elect. Dev., 52(9):43:19631969, 2005.